ARTICLE IN PRESS

npj Vaccines

https://doi.org/10.1038/s41541-026-01404-0

Article in Press

Structural insight into the assembly and D antigenicity of polio type 1 stabilized virus-like particles

Received: 30 September 2025

Accepted: 6 February 2026

Cite this article as: Hong, Q., Chen, T., Han, W. *et al.* Structural insight into the assembly and D antigenicity of polio type 1 stabilized virus-like particles. *npj Vaccines* (2026). https://doi.org/10.1038/s41541-026-01404-0

Qin Hong, Tian Chen, Wenyu Han, Shuxia Wang, Chaoyang Lian, Yujie Zhang, Lizhu Ruan, Tingfeng Wang, Cheng Lin, Congcong Song, Qingwei Liu, Xiaoli Wang, Yao Cong & Zhong Huang

We are providing an unedited version of this manuscript to give early access to its findings. Before final publication, the manuscript will undergo further editing. Please note there may be errors present which affect the content, and all legal disclaimers apply.

If this paper is publishing under a Transparent Peer Review model then Peer Review reports will publish with the final article.

ARTICLE IN PRESS

© The Author(s) 2026. **Open Access** This article is licensed under a Creative Commons Attribution-NonCommercial-NoDerivatives 4.0 International License, which permits any non-commercial use, sharing, distribution and reproduction in any medium or format, as long as you give appropriate credit to the original author(s) and the source, provide a link to the Creative Commons licence, and indicate if you modified the licensed material. You do not have permission under this licence to share adapted material derived from this article or parts of it. The images or other third party material in this article are included in the article's Creative Commons licence, unless indicated otherwise in a credit line to the material. If material is not included in the article's Creative Commons licence and your intended use is not permitted by statutory regulation or exceeds the permitted use, you will need to obtain permission directly from the copyright holder. To view a copy of this licence, visit http://creativecommons.org/licenses/by-nc-nd/4.0/.

ARTICLE IN PRESS

Structural insight into the assembly and D antigenicity of polio type 1 stabilized virus-like particles

Qin Hong[1,#], Tian Chen[2,#], Wenyu Han[3,4,#], Shuxia Wang[2], Chaoyang Lian[3,4], Yujie Zhang[2], Lizhu Ruan[3,4], Tingfeng Wang[2], Cheng Lin[1], Congcong Song[3,4], Qingwei Liu[3,4,*], Xiaoli Wang[3,4,*], Yao Cong[1,5,*], Zhong Huang[2,*]

[1] Key Laboratory of RNA Science and Engineering, Shanghai Institute of Biochemistry and Cell Biology, Center for Excellence in Molecular Cell Science, Chinese Academy of Sciences, University of Chinese Academy of Sciences, Shanghai, China.

[2] Shanghai Institute of Infectious Disease and Biosecurity, Shanghai Medical College, Fudan University, Shanghai, China

[3] Huasong (Shanghai) Biomedical Technology Co., LTD, Shanghai, China

[4] Chongqing Huazhi Biopharmaceutical Co., LTD, Chongqing, China

[5] Key Laboratory of Systems Health Science of Zhejiang Province, School of Life Science, Hangzhou Institute for Advanced Study, University of Chinese Academy of Sciences, Hangzhou, China

[#] Qin Hong, Tian Chen and Wenyu Han contributed equally to this article.

* Co-corresponding authors: Qingwei Liu (liuqingwei@huasongbio.com), Xiaoli Wang (xiaolliwang@huasongbio.com), Yao Cong (cong@sibcb.ac.cn), and Zhong Huang (huangzhong@fudan.edu.cn)

Running title: Structural mechanisms of PV1 sVLP assembly and D-antigenicity

ARTICLE IN PRESS

Abstract

The inherent instability of poliovirus capsids presents a formidable challenge for developing next-generation vaccines suitable for a post-eradication world. Here, we address this by engineering a thermally stabilized virus-like particle (sVLP) derived from the poliovirus serotype 1 (PV1) Mahoney-SC7 mutant and elucidating its atomic-level structure. Produced at remarkably high yields in *Pichia pastoris* yeast, our engineered sVLP maintains a native, D-antigenic conformation and elicits a potent neutralizing antibody response in mice, in sharp contrast to unstable wild-type VLP (wtVLP) which adopts an expanded, non-immunogenic form. Our 2.43 Å resolution cryo-EM structure reveals precisely how seven stabilizing mutations cooperatively enhance inter-protomer contacts and rigidify surface loops to lock the particle in its immunogenic state. We further define a critical D-antigenic epitope by determining the 2.60 Å structure of the sVLP in complex with a novel D-antigen-specific, neutralizing monoclonal antibody, 3G10, elucidating the structural mechanisms of D-antigen recognition and virus neutralization by 3G10. These findings provide a definitive structural blueprint for engineering stable, immunogenic vaccines for PVs and other enteroviruses and also deliver a vital reagent for ensuring vaccine quality control.

ARTICLE IN PRESS

ARTICLE IN PRESS

Introduction

Poliovirus (PV) is the causative agent of poliomyelitis, a contagious disease that may lead to paralysis or even death in young children [1]. As a member of the *Enterovirus* genus within the *Picornaviridae* family, PV possesses a single-stranded, positive-sense RNA genome of approximately 7.5 kb in length, packaged in a protein shell known as capsid [2-4]. The viral genome encodes a large polyprotein precursor that is subsequently processed into the structural protein P1 and the nonstructural proteins P2 and P3 [3]. P1 is further cleaved by a viral protease into capsid subunit proteins VP0, VP1, and VP3, with VP0 undergoing autocleavage during virion maturation to yield VP2 and VP4 [5-7]. It is well known that cell culture-derived PV exists in two particle forms: mature virion containing the viral RNA genome, and empty capsid (EC) lacking it. These two kinds of particles are distinct in antigenicity and immunogenicity [2,8]: PV native mature virions, the so-called D-antigen, are able to elicit protective immunity, whereas the naturally occurring ECs, also called C-antigen, fail to induce a protective immune response [4,9,10]. However, PV mature virion is thermally unstable, readily converting from D-antigen to C-antigen upon heating, resulting in a loss of protective immunogenicity [11,12]. These structural and antigenic distinctions underscore the need to understand PV capsid dynamics for developing stable, effective vaccines.

PV consists of three serotypes, namely PV1, PV2, and PV3 [1]. Currently used PV vaccines cover all three serotypes. These vaccines include the formaldehyde-inactivated polio vaccine (IPV) and the live attenuated oral vaccine (OPV) [1]. OPV is relatively inexpensive, easily administered, and capable of inducing both systemic and mucosal immunity. However, OPVs, especially OPV2, bear the risk of reverting to a neurovirulent form in vaccine recipients. This reversion can result in rare cases of vaccine-associated paralytic poliomyelitis (VAPP) and the generation of circulating vaccine-derived poliovirus (cVDPV) strains [1,13]. On the other hand, IPV can protect vaccinated individuals against poliomyelitis without reversion risk. However, it is unable to elicit robust mucosal immunity and therefore cannot adequately prevent virus shedding [14,15]. For both IPV and OPV, their manufacturing requires the growth and handling of a large amount of live infectious PV, posing risks of accidental release [16]. Clearly, currently used IPV and OPV have drawbacks in their manufacturing and application. These limitations highlight the urgent need for next-generation PV

ARTICLE IN PRESS

vaccines that eliminate live virus use in their production.

Virus-like particles (VLPs), produced in recombinant expression systems, offer a safe and effective platform for developing novel vaccines [17,18]. VLPs derived from the wildtype strain of PV (hereafter referred to as wtVLPs) have been previously generated in recombinant expression systems [19,20]. However, these VLPs, similar to naturally occurring ECs, are predominantly C-antigen and therefore poorly immunogenic [19,21]. By selecting virus mutants under increasing temperatures, Fox *et al.* identified stabilizing mutations in capsid subunit proteins across all three PV serotypes, which rendered the corresponding mutant ECs D-antigenic, thermally stable, and as immunogenic as the IPV counterparts [22]. Subsequently, these mutations enabled production of thermally stabilized VLPs (hereafter referred to as sVLPs) for all three PV serotypes in various recombinant expression systems [23-27]. The resulting sVLPs of each PV serotype are D-antigenic and efficiently induce neutralizing antibodies [23-27]. Structural studies show that the sVLPs of PV2 and PV3 adopt compact conformations resembling native mature virions [24,26,27], and elicit robust neutralizing antibodies, whereas wtVLPs exhibit an expanded state akin to naturally occurring ECs [23,25-27]. Recently, high-resolution structures of recombinant VLPs of a PV1 stabilized mutant termed SC6b (PV1-SC6b) were reported, revealing the presence of both D-particle and C-particle forms in the PV1-SC6b sVLP preparations [28].

Currently, measurement of D-antigen content in IPV vaccines relies on the use of D-antigen-specific monoclonal antibodies (mAbs) provided by the National Institute for Biological Standards and Control (NIBSC), including mAb234 for PV1, mAb1050 for PV2, and mAb520 for PV3. However, the molecular basis for their selective binding to the corresponding D-antigens over C-antigens remains unknown.

In this study, we produced both PV1 wtVLP and sVLP of another PV1 stabilized mutant, SC7, in *Pichia pastoris* yeast and comprehensively analyzed their antigenicity, thermostability, immunogenicity, and structure. We also identified a PV1 D-antigen-specific mAb, 3G10, and determined the cryo-EM structure of 3G10-bound PV1-SC7 sVLP. Our results not only show that the yeast-produced PV1-SC7 sVLP is a promising vaccine candidate with high-yield production

ARTICLE IN PRESS

capacity and desirable immunogenicity demonstrated in a mouse model, but also reveal structural mechanisms governing PV1-SC7 sVLP assembly and D-antigenicity.

Results

Expression and assembly of PV1 wtVLP and sVLP in *Pichia pastoris*

Building on our recent work with PV2 VLPs [23], we co-expressed the VP0, VP3, and VP1 proteins of PV1 in *Pichia pastoris* to generate VLPs. We constructed two vectors (termed PV1-wtVP^{031} and PV1-sVP^{031}), each of which contains three expression cassettes for VP0, VP3, and VP1 of the PV1 wildtype strain (Mahoney) or the thermo-stabilized mutant (Mahoney-SC7) [22], respectively (**Fig. 1a**). Each vector was transformed into the PichiaPink™ yeast and the resulting transformants were screened by ELISA with PV1-specific antibodies. After the high-expressing *P. pastoris* clones for both PV1-wtVP^{031} and PV1-sVP^{031} were identified, they were cultured, induced with methanol and subsequently subjected to a purification process as described in the Methods section. The purified materials from either the PV1-wtVP^{031}- or the PV-sVP^{031}-transformed yeast were analyzed by SDS-PAGE and western blotting with a set of three capsid subunit protein-specific antibodies (**Fig.1b**). For both the PV1-wtVP^{031} and the PV1-sVP^{031} samples, three protein bands of approximately 39 KDa, 36 KDa, and 29 KDa were detected by the VP0-specific, VP1-specific, and VP3-specific polyclonal antibodies, respectively (**Fig. 1b**), indicating co-expression and co-assembly of VP0, VP1 and VP3. Electron microscopy revealed the presence of spherical particles approximately 30 nm in diameter in both purified samples (**Fig. 1c**). Collectively, these data demonstrate that the VP0, VP3 and VP1 subunit proteins expressed in the PV1-wtVP^{031}- and PV1-sVP^{031}-transformed yeast were co-assembled into wtVLP and sVLP, respectively.

Antigenicity and thermostability of yeast-produced PV1 wtVLP and sVLP

The antigenicity of yeast-produced PV1 wtVLP and sVLP was assessed by ELISA using an anti-PV1 polyclonal antibody (pAb) and the D-antigen-specific mAb, mAb234. Both PV1 sVLP and wtVLP exhibited similar reactivity to the anti-PV1 sVLP polyclonal antibody. However, only the

ARTICLE IN PRESS

sVLP, but not the wtVLP, reacted in a dose-dependent manner with the mAb234 (**Fig. 2a**). These data indicate that only the sVLP, but not wtVLP, expresses D-antigen. To further quantify the D-antigen content in the sVLP preparations, a sandwich ELISA was performed using the international IPV standard (NIBSC code: 12/104) as a reference (**Supplementary Figure 1**). The analysis revealed that 1 μg of PV1 sVLP contained 187 units of D-antigen (**Fig. 2b**).

We next analyzed the thermostability of the PV1 sVLP. Aliquots of purified PV1 sVLP were heated for 10 minutes at temperatures ranging from 25°C to 60°C and then analyzed by ELISA. VLP samples stored at 4°C served as a positive control. As shown in **Fig. 2c**, the total antigen levels, as indicated by reactivity of the treated sVLP samples to the anti-PV1 pAb, remained roughly unchanged regardless of treating temperature. In contrast, the D-antigen content in the sVLP, measured by the binding activity to the mAb 234, remained stable up to 40°C but declined by more than 50% at 45°C.

PV1 sVLP, but not wtVLP, potently induces neutralizing antibody response

We evaluated the immunogenicity of PV1 wtVLP and sVLP by performing mouse immunization experiments. Groups of Balb/c mice (n=10) were immunized with either 1 μg or 4 μg doses of wtVLP or sVLP. A group receiving 0.5 dose of commercial IPV (containing 20 units of PV1 D-antigen) served as a positive control, while a group of mice administered PBS buffer served as the negative control. Sera were collected from individual mice after the second and third doses and analyzed for their neutralization potency (**Fig. 3a**). Due to limited access to wildtype PV1 strain, the attenuated vaccine strain, Sabin1 was used for the neutralization assays. As expected, none of sera from the control (PBS) mice exhibited any neutralizing activity. In contrast, 60% of the mice in the IPV group developed detectable neutralizing antibodies after the second dose, and all mice became sero-converted after the third dose, with a geometric mean neutralizing titer of 74 (**Fig. 3b**). For the wtVLP-immunized mice, neither the week-4 nor the week-6 sera exhibited neutralizaing activity, even at the lowest serum dilution (1:16) tested. In contrast, 80% and 100% of the mice in the 1-μg and 4-μg sVLP groups, respectively, were already sero-converted at week 4. After the third immunization, all mice in the 1-μg and 4-μg sVLP groups developed neutralizing

ARTICLE IN PRESS

antibodies with geometric mean titers being 169 and 239, respectively, at week 6 (**Fig. 3b**).

To further validate these findings, neutralization ability of the antisera was assessed using a GFP-expressing PV1 pseudovirus derived from the Sabin1 strain (**Fig. 3c** and **Supplementary Figure 2**). Consistent with the live virus assay, no neutralization was observed for any antisera from the control (PBS) or wtVLP-immunized mice. In contrast, for the IPV and the sVLP groups, the antisera's neutralizing titers detected by pseudovirus neutralization assay agreed well with the corresponding ones measured using the live virus (**Fig. 3b-c** and **Supplementary Figure 2**). Together, these results demonstrate that the sVLP, but not the wtVLP, potently elicits neutralizing antibodies.

Cryo-EM structures of PV1 wtVLP and sVLP

The structures of our PV1 wtVLP and sVLP were determined by cryo-electron microscopy (cryo-EM) single-particle analysis at resolutions of 2.95 Å and 2.43 Å, respectively (**Fig. 4a-b, Supplementary Figure 3, Supplementary Figure 4a-b,** and **Supplementary Table 1**). Both VLPs display an icosahedral architecture with surface features characteristic of enteroviruses, including a "mesa" situated at the 5-fold symmetry axes, a "canyon" surrounding the mesa, and a three-bladed propeller-like structure at the 3-fold axes (**Fig. 4a-b**). Notably, the radius of the wtVLP (170 Å) is larger than that of the sVLP (163 Å), indicating that wtVLP adopts an expanded conformation relative to the more compact sVLP (**Fig. 4a-b**). Moreover, an open channel is present at the 2-fold axes in wtVLP, while this channel is sealed in sVLP (**Fig. 4f**). Neither wtVLP nor sVLP showed any density corresponding to RNA within the capsid (**Fig. 4c-d**).

Atomic models were built for both maps, showing good fit to their respective cryo-EM maps and revealing high-resolution structural details (**Fig. 4e**). The 2-fold axis channel, which is formed by VP2 and VP3, is markedly open in wtVLP but sealed in sVLP (**Fig. 4f**). Importantly, both wtVLP and sVLP contain empty hydrophobic pockets within VP1 (**Supplementary Figure 4c**). Structural comparisons with previously reported poliovirus structures (PV1 mature virion, PDB: 1HXS [29], and PV1 expanded 135S particle, PDB: 6P9O [30]) revealed that wtVLP closely resembles the PV1 135S-like particles (RMSD = 0.741 Å), while the sVLP aligns well with the native PV1 structure

ARTICLE IN PRESS

(RMSD = 0.600 Å) (**Supplementary Figure 4g-h**). These results indicate that PV1 sVLP adopts a native conformation similar to that of the corresponding mature virion, whereas the PV1 wtVLP is in a non-native expanded state.

For both wtVLP and sVLP, the overall structures of VP1, VP2, and VP3 proteins are similar, each characterized by an eight-stranded antiparallel β-barrel core (**Supplementary Figure 4d-e**). However, key structural differences are observed in the VP1 β-barrel pocket, loop regions, and the N- and C-termini of the proteins. Specifically, the VP1 N-terminus in sVLP appears more stable and better resolved, starting from R24, whereas in wtVLP it is disordered until S71 (**Supplementary Figure 4d**). Moreover, the GH loop of VP1 and the EF loop of VP2 are well-ordered in sVLP but flexible in wtVLP (**Supplementary Figure 4d-e**). Loops connecting the β-barrel domains, particularly those at the 5-fold, 3-fold, and quasi-3-fold axes, undergo distinct conformational changes (**Supplementary Figure 4d-f**).

Compared to the wtVLP, our sVLP, which is derived from the PV1-SC7 mutant, carries seven amino acid substitutions: VP1 V196L, VP1 H248P, VP2 T25A, VP2 D57E, VP3 Q178L, VP3 L119M, and VP4 R18G (**Fig. 5a**). These mutations have previously been implicated in stabilizing PV1 empty capsids [22]. According to our models, the H248P substitution in the VP1 HI loop alters surface charge and induces conformational changes in the adjacent BC and HI loops (**Supplementary Figure 4i-j**). The V196L substitution in the VP1 pocket of sVLP shifts the pocket outward, increasing the distance between residue 196 and Y159 from 3.4 Å to 4.7 Å (**Supplementary Figure 4k**). Meanwhile, the Q178L mutation in VP3, located at the quasi-3-fold axis, triggers a conformational shift in the VP1 GH loop of the adjacent protomer, enhancing inter-protomer packing (**Supplementary Figure 4l**). Collectively, these mutations promote a more compact packing both within and between protomers (**Supplementary Figure 4m**).

The cryo-EM structures of the sVLP of another PV1 stablizing mutant, termed SC6b, have recently been determined, revealing the presence of both D and C Ag particle forms [28]. Structural comparisons shows that our SC7 sVLP structure aligns well with the SC6b D particle (PDB: 9EYY), with an RMSD of 0.703 Å (**Fig. 5b**), but not with the SC6b C particle (PDB: 9EZ0), for which the

ARTICLE IN PRESS

RMSD across all pairs is 1.928 Å. Detailed analysis indicates that the individual VP1, VP2, and VP3 subunits of SC7 and SC6b D-particles are nearly perfectly superimposable, with only minor deviations observed in the BC and DE loop of VP1 (**Fig. 5c-e**). Notably, the VP1 pocket in SC7 sVLP is smaller than in the SC6b D particle (**Fig. 5f**), likely due to the V196L substitution in SC7, which introduces a bulkier side chain that may strengthen interactions with neighboring residues and render the overall conformation more compact (**Fig. 5f**).

In contrast, our PV1 wtVLP closely resembles the yeast- or mammalian cell-produced SC6b C particles, with RMSDs of 0.870 Å and 0.807 Å, respectively (**Fig. 5g-h**), and differs significantly from the yeast-produced SC6b D particle (RMSD across all pairs =1.976 Å). This observation confirms the expanded conformation of wtVLP and explains its lack of D antigenicity (**Fig. 2a-b**). Compared with PV1 SC6b yeast and mammalian C particles, the VP1 loops of wtVLP adopt a distinct conformation at the 5-fold axis, and the N terminus of its VP3 appears less stable (**Fig. 5g-h**).

Identification of mAb 3G10 as a PV1 D-antigen-specific antibody

To further characterize the antigenic sites on PV1 VLPs, we attempted to isolate PV1-specific mAbs by using traditional hybridoma technology. Splenocytes from PV1 sVLP-immunized mice were fused with SP2/0 myeloma cells, and the resulting hybridomas were screened for PV1 sVLP binding by ELISA. Finally, two hybridoma clones secreting PV1 sVLP-binding antibodies were identified and designated 3G10 and 5C6 (**Fig. 6a-b**). Isotyping assay showed that 3G10 and 5C6 were of IgG2a and IgG2b isotypes, respectively (**Fig. 6a**). Sequence analysis confirmed that they are indeed distinct antibodies (**Supplementary Figure 5a**). To evaluate their binding specificity, ELISA assays were performed using various capture antigens. As shown in **Fig. 6b-c**, 5C6 bound both PV1 sVLP and wtVLP in an antigen dose-dependent manner, whereas 3G10 recognized only PV1 sVLP. Neither 3G10 nor 5C6 reacted with PV2 sVLP or wtVLP (**Supplementary Figure 5b**), indicating that both mAbs are PV1-specific.

The observation that 3G10, like the known D-antigen-specific mAb234, binds exclusively to PV1 sVLP but not to wtVLP suggests that 3G10 also targets a D-antigenic epitope. To confirm

ARTICLE IN PRESS

this, we used both mAb234 and 3G10 in parallel to probe the thermostability of PV1 sVLP. As shown in **Fig. 6d**, both antibodies detected a drastic reactivity decrease when sVLP sample were heated to 45°C, further supporting the classification of 3G10 as a PV1 D-antigen-specific mAb. BLI analysis revealed that 3G10 exhibited high binding affinity to the D-antigenic PV1 sVLP with an equilibrium dissociation constants (KD) of 0.53 nM (**Fig. 6a** and **6e**).

To investigate whether the three mAbs (3G10, 5C6, and mAb234) target the same or overlapping sites in the capsid, we performed competitive ELISA using PV1 sVLP as the coating antigen. In this assay, immobilized PV1 sVLP was firstly incubated with serially diluted mAbs (1st mAb), followed by detection with HRP-conjugated 3G10 (designed 3G10-HRP). As shown in **Fig. 6f-g**, pre-incubation with unconjugated 3G10 inhibited subsequent binding of 3G10-HRP onto PV1 sVLP in a dose-dependent manner. In contrast, neither 5C6 nor an irrelevant mAb showed any inhibition regardless of the antibody concentration, indicating that 3G10 and 5C6 have distinct binding sites. Notably, pre-incubation with mAb234 also dose-dependently inhibited 3G10-HRP binding (**Fig. 6g**), suggesting that 3G10 and mAb234 target the same or highly overlapping epitopes whilst 5C6 binds a distinct site.

The neutralization capacity of 3G10 and 5C6 was firstly assessed using pseudovirus neutralization assays. 3G10 showed potent neutralizing activity against both Sabin-1 and Mahoney strain-derived pseudovirus, with IC90 values of 0.006 μg/mL. In contrast, 5C6 exhibited only weak neutralization, with IC90 values of 25 μg/mL against both Sabin-1 and Mahoney pseudoviruses (**Fig. 6a** and **Supplementary Figure 5c**). The neutralization ability of the two mAbs was verified by performing Sabin-1 live virus neutralization assays. Consistent with the pseudovirus neutralization data, 3G10 effectively neutralized the live virus with an IC50 of 0.016 μg/mL, while 5C6 exhibited poor neutralization activity (IC50=18.75 μg/mL). Together, these results identify 3G10 as a potent PV1 D-antigen-specific mAb that binds a neutralizing antigenic site shared with mAb234.

Structure of 3G10-bound PV1 sVLP

To elucidate the molecular basis of 3G10's specific recognition of PV1 sVLP but not wtVLP, we

ARTICLE IN PRESS

determined the cryo-EM structure of the sVLP in complex with the 3G10 Fab fragment at a nominal resolution of 2.60 Å (**Fig. 7a, Supplementary Figure 6a**). 2D classification of the sVLP-3G10 Fab complex revelaed high Fab occupancy on the sVLP capsid, in contrast to free sVLP (**Supplementary Figure 3b-c**). Structural analysis revealed that 3G10 Fabs bind at the apices of the canyon of sVLP, forming a star-like configuration around the 5-fold axis (**Fig. 7a-b**). Focused refinement of the VP1/2–3G10 Fab region yielded a map at a resolution of 2.83 Å (**Supplementary Figure 3c, Supplementary Figure 6b**), with the majority of the side-chain densities well resolved, allowing for accurate atomic model building (**Fig. 7b**). The atomic model of the sVLP–3G10 complex fits the cryo-EM density well (**Fig. 7b**).

The 3G10 heavy chain plays the dominant role in antigen recognition, contributing more extenively to interactions with VP1/2 than the light chain (**Fig. 7c-d**). All three heavy-chain complementarity-determining regions (CDRs) of 3G10, along with its CDRL1 and CDRL3 from the light chain, engage primarily with the VP1 GH loop and the VP2 EF loop. Notably, the EF loop is dynamic in wtVLP but appears stabilized upon 3G10 binding in sVLP (**Fig. 7d,** and **Fig. 5c-d**). CDRH2 and CDRH3 form multiple hydrogen bonds and salt bridge with the VP1 GH loop and VP2 EF loop, while CDRH1 and N-terminal region of 3G10 establish hydrogen bonds with the VP1 BC loop (**Fig. 7d, Supplementary Table 2**), thereby establishing an extensive interaction network between the 3G10 Fab and VP1/2. Additional interactions were observed between 3G10 and the VP3 subunit of a neighbouring protomer (**Supplementary Table 3**), further stabilizing the complex. Importantly, 3G10 binding induces only minor conformational changes in VP2 EF loop$_{135-143}$ and VP1 GH loop (**Fig. 7e**), suggesting that the epitope is preformed and structurally stable in sVLP.

These results identify the VP2 EF loop, as well as the VP1 BC and GH loops, as key epitopes for 3G10 binding. The 3G10 Fab docks into the sVLP canyon, with the heavy chain tilted toward the 5-fold axis, effectively obscuring the canyon region (**Fig. 7c-d**), which is involved in receptor binding [31] (**Fig. 7f**). The 3G10 epitope overlaps almost entirely with the poliovirus receptor (PVR, or CD155) binding site (**Fig. 7f**), leading to steric hindrance that would block receptor engagement

ARTICLE IN PRESS

(**Supplementary Figure 6d**). This mechanistic insight explains the potent neutralizing activity of 3G10 (**Fig. 6a**).

A sandwich ELISA based on the 3G10/5C6 mAb pair for measurement of PV1 D-antigen

It is well recognized that D-antigen is the protective antigen component of any IPV vaccines. Although mAb234 supplied by the NIBSC has long been used as the detection antibody in ELISAs to measure PV1 D-antigen content in wildtype strain-based conventional IPV (cIPV) vaccines, its binding epitope remains obscure thus far. We therefore evaluated whether the structurally defined 3G10 could serve as an alternative detection mAb for PV1 D-antigen quantification.

We first assessed conservation of the 3G10 epitope by sequence alignment. As shown in **Fig. 8a**, all contact residues of the 3G10 epitope are identical among the Mahoney-SC7, the wildtype Mahoney, and Sabin-1 strains, supporting the potential broad applicability of 3G10 in D-antigen ELISAs for PV1 sVLPs, cIPVs, and Sabin strain-derived IPVs (sIPVs).

To verify our hypothesis, we performed sandwich ELISAs using a rabbit anti-PV1 polyclonal antibody (pAb) as the capture antibody, different mAbs as detection antibodies, and the international cIPV standard (NIBSC code: 12-104) as the reference. As shown in **Fig. 8b**, 3G10 yielded a reactivity curve nearly identical to that of mAb234, indicating that 3G10 detects PV1 D-antigen as efficiently as mAb234 in ELISA. Similarly, mAb 5C6 also reacted with the cIPV standard in a dose-dependent manner. Because the rabbit anti-PV1 pAb capture antibody may not be consistent among batches due to limited supply for each batch, we next optimized the D-antigen sandwich ELISA assay using matched mAb pair.

We selected 5C6 as the capture antibody because it binds both PV1 wtVLP and sVLP (**Fig. 6b-c**), enabling capture of both C- and D-antigenic particles. 3G10, which does not compete with 5C6 (**Fig. 6f**), was conjugated with horseradish peroxidase (HRP) and used as the detection antibody. In this double-mAb sandwich ELISA, OD450 values correlated well with input D-antigen (**Fig. 8c-d**), validating the 5C6/3G10-HRP based sandwich ELSA for measurement PV1 D-antigen content in candidate vaccines.

ARTICLE IN PRESS

Discussion

PV sVLPs, recombinant VLPs derived from the thermostabilized PV mutants, represent a promising strategy for the development of new-generation non-replicating PV vaccines to replace current IPVs [22,24,26,27]. A detailed understanding of their antigenic and structural characterization is crutial for the product development of sVLP-based PV vaccines. Here, we report high-yield production of PV1 wtVLP and PV1-SC7 sVLP in *P. pastoris* yeast and provide a comprehensive analysis of their antigenicity, immunogenicity, and structures. Our study also delivers, to the best of our knowledge, the first near-atomic-resolution structure of a PV1 sVLP in complex with a potently neutralizing, D-antigen-specific antibody.

By simultaneously co-expressing VP0, VP3, and VP1–a unique expression strategy developed in our group [23], we achieved high-yield production of PV1-SC7 sVLP in *P. pastoris* yeast, obtaining around 1.2 milligram of purified sVLP per gram of yeast wet weight. Importantly, the purified sVLP is D-antigenic, possessing approximately 187 DU per μg protein. This corresponds to ~224,400 DU per gram of the engineered yeast, equivalent to 5,610 human doses (40 DU per dose for PV1) of commercial IPV vaccines. Two other expression strategies have previously been employed to produce PV1-SC6b D-antigenic sVLP in yeast, including co-expression of P1 and an uncleavable 3CD [32] and co-expression of VP3-P2A-VP0 and VP1 or VP3-P2A-VP1 and VP0 [33]. Specifically, Sherry *et al.* reported that the level of PV1 D-antigen yield achieved by co-expressing P1 and uncleavable 3CD of PV1-SC6b was ~1000 DU per 100 ml yeast culture while approximately 3-fold or 5-fold less D-antigen was obtained when the 30-1 contruct (co-expressing VP3-P2A-VP0 and VP1) or the 31-0 construct (co-expressing VP3-P2A-VP1 and VP0) was used, respectively [33]. Based on these data, our three-cassette construct, which allows simultaneous expression of tag-free VP0, VP3 and VP1, appears to be much more efficient than the other two strategies in terms of the final PV1 D-antigen yields achieved. We reason that, aside from the slight difference (one amino acid change) in the sVLP sequence, several unique traits of our expression strategy may have contributed to the high-level production of PV1 D-antigen. Firstly, our strategy does not involve the expression of 3CD protease and therefore eliminates 3CD-

ARTICLE IN PRESS

caused cellular toxicity and/or incomplete cleavage of P1 by 3CD. Secondly, our strategy precisely expresses tag-free VP0, VP3 and VP1, hence permitting efficient and authentic sVLP assembly in the D-antigenic conformation; in contrast, it has been shown that, when one of VP0, VP3 and VP1 was tagged with P2A or 6xHis, the formation of D-antigen particle was negatively affected to different degrees [33]. Taken together, the results of the present study and previously published works suggest that the VP0/VP3/VP1 co-expression strategy is optimal for achieving high-yield production of D-antigenic PV sVLPs in yeast.

In addition to yeast, other recombinant expression systems including plant, insect cell, and mammalian cell have been used to produce PV sVLPs [23-27]. Recently, Sherry et al. performed a comparative analysis of PV sVLPs produced by co-expressing of P1 and 3CD in different recombinant systems [28]. The study shows that yeast is in general comparable to the baculovirus/insect cell system but superior to the plant and MVA/mammalian cell systems in terms of D-antigen yield [28]. In particular, for PV1-SC6b, the D-antigenic sVLP yields under laboratory conditions were 1030, 398 to 969, 26.3 DU per 100 ml culture in the yeast, insect cell, and mammalian cell systems, respectively, and 235 DU per 10 gram leaf material in the plant system [28]. It is possible that optimization of yeast fermentation methods and conditions may further increase PV sVLP yields. Indeed, through controlled fermentation, the yield of PV1-SC6b D-antigen in yeast can be increased by approximately 3-fold [32]. More significantly, by employing the VP0/VP3/VP1 co-expression strategy, we achieved high-level production of D-antigenic PV sVLPs in yeast, with yields of around 673,200 DU (equivalent to 16,830 human doses) per 100 ml culture for PV1-SC7 (**Fig. 2b**, based on 3 gram yeast wet weigh per 100 ml culture) and 4398 DU (equivalent to 550 human doses) per 100 ml culture for PV2-SC5a [23]. Such a high-yield production capacity highlights the advantage of yeast-produced sVLPs as a cost-effective vaccine source for global mass vaccination in the future.

Mouse immunization experiments confirmed that the PV1 sVLP, but not the wtVLP, is highly immunogenic (**Fig. 3**). Specifically, the mice immunized with either 1-μg or 4-μg of PV1 sVLP elicited higher neutralizing antibody titers exceeding those induced by 0.5 human dose (20 DU for

ARTICLE IN PRESS

PV1) of commercial IPV after the third dose, whilst no neutralizing antibody response was detected by PV1 wtVLP. Our immunogenicity study has several limitations. Firstly, the 1-μg and 4-μg PV1 sVLP doses tested in the study contain 187 and 748 DU, respectively, which are much higher than a single human dose (40 DU) of commercial IPV, making it difficult to directly compare the immunogenicity of sVLP and IPV. Secondly, our immunogenicity analysis was performed on mice, rather than on Wistar rats which are the standard animal model for IPV vaccine batch release. In the future, additional immunization experiments using equal D-antigen doses of sVLP and IPV should be conducted in both mice and rats to more precisely determine the immunogenic potency of PV1 sVLP.

At the time when this study was initiated, no high-resolution structure of PV1 sVLP was available. Recently, Sherry *et al*. reported the cryo-EM structures of PV1-SC6b sVLP produced in yeast or expressed via MVA at 3.3 Å or 3.0 Å resolution, respectively [28]. In this study, we determined the cryo-EM structure of yeast-produced sVLP of another mutant, PV1-SC7, at 2.43 Å resolution, as well as the 2.95 Å structure of PV1 wtVLP. Our structure analysis shows that the PV1 wtVLP is in a more expanded state with an open channel at the 2-fold axis, while this channel is sealed in the PV1-SC7 sVLP. The PV1-SC7 sVLP harbors seven stabilizing amino acid substitutions, such as VP1 V196L, VP1 H248P, and VP3 Q178L, which enhance PV1 empty capsid stabilization. For example, the VP1 H248P mutation alters the surface charge of the VP1 HI loop, inducing conformational changes in the BC and HI loops (**Supplementary Figure 4i**), while the VP3 Q178L mutation at the quasi-3-fold axis alters the VP1 GH loop conformation of the neighboring protomer (**Supplementary Figure 4l**). The PV1-SC7 sVLP exhibits a more stable VP1 N-terminus and structurally more rigid VP1 GH loop and VP2 EF loop compared to the wtVLP (**Supplementary Figure 4d-e**). These features make the PV1-SC7 sVLP more thermostable than the wtVLP and resemble the conformation of the native mature virion (the so-called “D Ag particle”) (**Supplementary Figure 4g-h**). Notably, yeast-derived PV1-SC6b sVLPs contains both D and C Ag particles (ratio ~1:1.8), whereas MVA-expressed PV1-SC6b sVLPs are predominantly non-immunogenic C Ag particle form [28]. In sharp contrast, our cryo-EM analysis reveals that all yeast-

ARTICLE IN PRESS

produced PV1-SC7 sVLPs examined are D Ag particles. Collectively, these data suggest that PV1-SC7 sVLP is superior to PV1-SC6b sVLP as a vaccine candidate for PV1.

The only difference between PV1-SC6b and PV1-SC7 is an additional mutation, V196L of VP1, in PV1-SC7, implicating a significant role of the VP1 V196L in PV1 capsid stabilization and D Ag particle formation. Indeed, detailed structural analysis reveals that the VP1 V196L substitution introduces a bulkier side chain, leading to a shrunk hydrophobic pocket and strengthened inter-protomer contacts (**Fig. 5f**), which may ultimately result in more robust stabilization of D Ag particle.

We also identified and characterized a PV1 D-antigen specific mAb termed 3G10. Our 2.60-Å-resolution structure of the 3G10-sVLP complex provide the atomic-resolution view of a D-antigen-specific mAb bound to a poliovirus D Ag particle. 3G10 specifically binds PV1 sVLP but not wtVLP (**Fig. 6**), driven by the enhanced stability of sVLP and conformational differences in key epitopes between sVLP and wtVLP. The binding sites of 3G10 are mainly concentrated on the VP1 BC and GH loops and the VP2 EF loop (**Fig. 7d**), which exhibit stable conformations in sVLP but are more dynamic in wtVLP (**Supplementary Figure 4d-e**). Specifically, the heavy chain of 3G10 predominantly interacts with VP1/2 than the light chain, forming an extensive hydrogen bond and salt bridge network via its three CDRHs with the VP1 GH and VP2 EF loop. This binding mode is stable in sVLP, but is difficult to achieve in wtVLP due to epitope instability.

Three major neutralizing antigenic (N-Ag) sites have been previously described for PVs [34-39]. The newly identified 3G10 epitope involves amino acid residues from both N-Ag I and II sites, including VP1 GH-loop residues (Ser221, Asp226, Leu228), VP2 EF-loop residue (Thr168) from N-Ag II site, and VP1 BC-loop residues (Asn100, Lys101, Asp102) and EF-loop residue (Glu168) from N-Ag I site (**Supplementary Table 2 and 3**), therefore suggesting that 3G10 targets a novel N-Ag site which is more complexed than the classical N-Ag sites I to III. Interestingly, the 3G10 epitope extensively overlaps the binding site of a human mAb, 9H2 [35,36] (**Supplementary Figure 6c**), despite, unlike 3G10, 9H2 neutralizes all three PV serotypes and binds to both D-Ag and C-Ag particle forms[40]. Thus, together, 3G10 and 9H2 define the fourth N-Ag site on the PV capsid.

ARTICLE IN PRESS

Binding footprint analysis shows that the 3G10 epitope highly overlaps the PVR receptor binding site (**Fig. 7f**), suggesting that 3G10 exerts neutralization via steric hinderance of PVR binding. Notably, the 3G10 epitope is conserved across PV1-SC7, wildtype Mahoney strain, and attenuated Sabin-1 strain (**Fig. 8a**). This is in consistence with the nearly equal neutralization potency of 3G10 towards Mahoney and Sabin-1 pseudoviruses (**Fig. 6a** and **Supplementary Figure 5c**). Thus, 3G10 may serve as a universal detection antibody for D-antigen quantification for not only PV1 sVLPs, but also the commercial Mahoney- or Sabin-1-based IPVs. It should be noted that, although the D-antigen-specific mAbs such as 3G10 are suitable for antigenic analysis of PV vaccine candidates, they cannot directly measure immunogenicity.

In summary, our study establishes yeast-produced PV1-SC7 sVLP as a high-yield, optimal recombinant PV1 vaccine candidate, and identies a PV1 D-antigen-specific mAb, 3G10, as a structurally defined reagent for quality control of different forms of PV1 vaccines. High-resolution cryo-EM analysis further elucidates the molecular mechanisms of PV1-SC7 sVLP assembly and D-antigenicity, accelerating sVLP-based PV vaccine development.

ARTICLE IN PRESS

ARTICLE IN PRESS

Methods

Cells

293T cells (National Collection of Authenticated Cell Cultures, Shanghai, China) were cultured in Dulbecco's modified Eagle's medium (DMEM) supplemented with 10% fetal bovine serum (FBS) and 100U/mL penicillin-streptomycin (Gibco) at 37°C with 5% CO_2. PichiaPink™ yeast strains (Invitrogen, USA) were grown according to the manufacturer's instruction.

Antibodies

The mAb 234 was purchased from the National Institute for Biological Standards and Control (NIBSC), UK. The anti-VP2, anti-VP3 and anti-VP1 polyclonal antibodies were generated in house by immunization of rabbits with recombinant PV1 VP2, VP3 or VP1 protein produced from *Escherichia coli* as previously reported [41], respectively. The rabbit polyclonal antibodies against PV1 VLP was generated in house by immunization of rabbits with PV1 wtVLP plus Freund's adjuvant (Sigma, St. Louis, MO, USA). The PV2-specific mouse monoclonal antibody 1G3 was described previously [23].

Construction of yeast expression vectors

The P1 coding sequences for PV1 wildtype strain Mahoney (Gene Bank: KU866422.1) and the Mahoney-SC7 mutant were optimized for yeast expression and synthesized by Genscript (Nanjing, China). The VP0, VP1 and VP3 fragments of the optimized PV1 wtP1 gene were amplified by PCR and clone into pPinK-HC vector (Invitrogen) using ClonExpress Ultra One Step Cloning kit (Vazyme, China), yielding plasmids HC-wtVP0, HC-wtVP1, and HC-wtVP3, respectively. The wtVP3 and wtVP0 expression cassettes were released from HC-wtVP0 and HC-wtVP3 by BamH I and Bgl II digestion, respectively, and then sequentially inserted into HC-wtVP1 from Bgl II site, yielding plasmid HC-wtVP^{031} that contained all three (wtVP0, wtVP3, wtVP1) expression cassettes. In the same way, plasmid HC-sVP^{031} that contained sVP0, sVP3 and sVP1 expression cassettes was constructed.

ARTICLE IN PRESS

Pichia pastoris transformation and selection of high-expression clones

Prior to *P. pastoris* transformation, plasmids HC-wtVP^{031} or HC-sVP^{031} was linearized by digestion with *Afl* II. PichiaPink™ Strain 1 (Invitrogen) was transformed with the linearized plasmids and subsequently plated onto PAD plates as previously described [42]. Individual yeast colonies were randomly picked from the plates and small-scale expression experiments were performed according to the manufacturer's instruction (Invitrogen). Induced yeast cells were harvested and lysed. Total soluble protein (TSP) in the clarified lysates were measured with Coomassie Plus Protein Assay Reagent (Thermo). VLP expression in the clarified lysates was determined by ELISA as described below. Briefly, lysate containing 25μg or 50μg TSP was added to wells of the 96-well ELISA plates and then incubated at 37°C for 2 hr; after three washes with PBST buffer, wells were blocked with 5% milk diluted in PBST overnight at 4°C; after three washes, mAb234 (diluted 1:1000 in 2% milk/PBST) or anti-PV1 sVLP mouse sera (diluted 1:2000 in 2% milk/PBST) was added and incubated at 37°C for 2 hrs; after three washes, 50μl of HRP-conjugated goat anti-mouse IgG (Sigma) was added to each well and incubated at 37°C for 1 hr; after 5 washes, color was developed with TMB substrate (Thermo Fisher), and the absorbance at 450nm was measured.

ARTICLE IN PRESS

Preparation of VLP antigens

To prepare VLP antigens, the selected yeast strains were grown and then induced for antigen expression with methanol according to the manufacturer's instruction (Invitrogen). The induced yeast cells were pelleted and suspended in 0.15M phosphate buffered saline (PBS) buffer. The cells were then lysed using a high-pressure cell disrupter (JNBIO, China) at 1,800 Bar, and the resultant crude lysates were clarified by centrifugation at 12,000 rpm for 15 min. Then, NaCl and PEG 8000 were added into the clarified lysates to reach final concentrations of 200 mM and 10% (W/V), respectively, and the mixtures were stirred gently at 4°C overnight to allow protein precipitation. Next day, the mixtures were subjected to centrifugation at 12,000 rpm for 15 min, and the resultant pellets were resuspended in PBS buffer, followed by centrifugation at 12,000 rpm for 15 min to remove insoluble fractions. The clarified supernatants were then subjected to

ARTICLE IN PRESS

ultracentrifugation at 27,000 rpm for 4 hrs on a 20% sucrose cushion. The resultant pellets were resuspended in PBS and then layered onto 10-50% sucrose gradients for ultracentrifugation at 39,000 rpm for 3 hrs. Twelve fractions were taken from top to bottom and assayed. Based on the SDS-PAGE and Western blotting results, VLP-rich fractions were pooled and then pelleted by ultracentrifuging through a 20% sucrose cushion. The pelleted VLPs were resuspended in PBS, quantified by Bradford assay, and then stored at -80°C until use.

SDS-PAGE and Western blot assays

Protein samples were analyzed by electrophoresis on 12% polyacrylamide gels, followed by staining with Coomassie blue. For Western blot assays, protein on unstained SDS-PAGE gels was transferred onto PVDF membranes. The membranes were probed with an antigen-specific primary antibody, followed by a corresponding HRP-conjugated secondary antibody. Western blots were developed using BeyoECL Plus kit (Beyotime, Shanghai, China) and then imaged digitally.

Negative stain electron microscopy

Purified VLP samples were subjected to negative staining with 0.5% aqueous uranyl acetate, followed by transmission electron microscopy using a Tecnai G2 Spirit microscope operated at 120 KV.

ELISA

The antigenicity of VLPs was assessed by performing indirect ELISAs. Briefly, wells of 96-well microtiter plates were coated with the protein samples (50 µl/well) at 4°C overnight; then the plates were washed three times with PBST buffer after each of the following steps. Consecutively, 200 µl/well of 5% milk in PBST was added for blocking and incubated at room temperature (approximately 20-25°C) for 1 hr; 50 µl/well of a primary antibody in PBST plus 1% milk was added and incubated at room temperature for 2 hrs; then 50 µl/well of a corresponding HRP-Conjugated

ARTICLE IN PRESS

secondary antibody in PBST plus 1% milk was added and incubated at room temperature for 1 hr. For color development, 50µl/well TMB mixture was added and incubated for 5-10 minutes; then 1M H_3PO_4 was added to stop the reaction. Absorbance was measured at 450nm in a 96-well plate reader.

D antigen content in protein samples was quantitated by sandwich ELISA. Briefly, wells of 96-well ELISA plates were coated with 50 µl of rabbit anti-PV1 polyclonal antibody (diluted 1:4000 in PBS) at 4°C overnight; after three washes with PBST buffer, plates were blocked with 5% milk diluted in PBST for 1 hr; after three washes, protein samples to be tested or the international IPV standard (NIBSC code: 12-104) diluted in 2% milk/PBST were added and incubated at room temperature for 2 hr; then, 50 µl/well of PV1-specific mAb234 (diluted 1:1000 in PBS) were added and incubated at room temperature for 2 hr; at last, 50 µl/well of a corresponding HRP-Conjugated secondary antibody in PBST plus 1% milk was added and incubated at room temperature for 1 hr. Color development and absorbance measurement were carried out as described above. The D antigen content for each test sample was evaluated against the IPV standard with assigned D antigen units.

Competitive ELISA was performed to investigate the epitope competition among PV1 mAbs. 3G10 was conjugated to HRP using the EZ-Link™ Plus Activated Peroxidase Kit (Thermo Scientific, Cat# 31489) according to the manufacturer's instructions. Wells of ELISA plates were coated with PV1 sVLP (100 ng/well) and then incubated with serial dilutions of the primary competing mAbs or with 2% milk/PBST as the negative control for 1 h at room temperature. Subsequently, 50 ng/well of HRP-conjugated 3G10 was added, followed by incubation for 1 h at room temperature. After washing, TMB mixture was added to wells for color development and absorbance was measured as described above.

Thermostability analysis.

For the temperature escalation experiment, aliquots of 25 ng of PV1 sVLP were incubated for 10 mins at a range of temperatures from 25°C to 60°C and then cooled on ice. Then, the samples

ARTICLE IN PRESS

were analyzed by ELISA as described above.

Mouse immunization study

The animal studies were approved by the Institutional Animal Care and Use Committee at Youshu Life Technology (Shanghai). Balb/c mice used in this study were purchased from Laboratory Animal Center of Shanghai Lingchang Biotechnology. The mice were kept in the specific pathogen free animal facility of Youshu Life Technology with controlled temperature (20-26°C), humidity (40-70%), and lighting conditions (12 h light/12 h dark cycle).

Prior to immunization, antigens were diluted with PBS to make the experimental vaccines. A single injection dose contained 1 or 4 μg of PV1 wtVLP or sVLP without adjuvant, or half human dose of commercial IPV vaccine (20 DU for PV1, Sanofi Pasteur) in a final volume of 500 μl, respectively.

Groups of 9-10 female Balb/c mice (6-8 week) were injected intraperitoneally (i.p.) with one of the experimental vaccines at week 0, 2 and 4. Blood samples were collected at week 4 and week 6. The resulting mouse sera were incubated at 56 °C for 30 min to inactivate the complement and then stored at -80°C until use. At the end of the experiment, all mice were euthanized humanely using carbon dioxide inhalation followed by cervical dislocation.

ARTICLE IN PRESS

Live virus neutralization assay

The live virus neutralization assay was conducted in a 96-well plate as described in Chinese Pharmacopoeia (2025 edition). Briefly, 50 μl of serially diluted serum (two-fold dilutions) were mixed with an equal volume of PV1/Sabin1 live virus (32~320 $TCID_{50}$ per well). The mixture was incubated at 37°C for 2 h and then at 4°C overnight. Subsequently, 1.5×10^4 Hep-2 cells were added to each well, and the plate was incubated at 37°C with 5% CO_2. After 7 days, the cells were microscopically examined for cytopathic effects (CPE). The neutralization titers were defined as the highest serum dilution that protected 50% the cell cultures from CPE.

Preparation of PV1 pseudovirus

ARTICLE IN PRESS

PV1 pseudovirus was generated by co-transfecting 293T cells with three plasmids, including P1-expressing plasmid, replicon plasmid, and T7 polymerase-expressing plasmid. The PV1/Sabin1 capsid protein gene P1 (GenBanck: AY184219) or PV1/Mahoney capsid protein gene P1 (GenBanck: KU866422.1) linking with the dsRed gene via a 2A cleavage signal sequence were synthesized by Genscript (Nanjing, China) and cloned into pCDNA3.3 (Thermo), generating the P1-expressing plasmid designated pcDNA3.3-dsRed/Sabin1-P1 and pcDNA3.3-dsRed/Mahoney-P1, respectively. The DNA sequence of the PV1/Mahoney genome (GenBanck: V01149) with its P1 gene replaced by eGFP was synthesized by Genscript and cloned downstream the T7 promoter, yielding the RNA replicon vector designated pT7-Replicon-eGFP. The T7 polymerase (GenBanck: M38308) was also synthesized by Genscript and cloned into pcDNA3.3, yielding the T7 polymerase-expressing plasmid pcDNA3.3-T7.

For pseudovirus production, 293T cells were seeded into 6-well plates at a density of $2x10^5$ cells/ well and incubated at 37°C with 5% CO_2 the day before transfection. Cells at 20~30% confluency were transfected with 3 μg pcDNA3.3-dsRed/Sabin1-P1 or pcDNA3.3-dsRed/Mahoney-P1 formulated with Lipo3000 transfection reagent (Invitrogen), and 2 μg pcDNA3.3-T7 and 2 μg pT7-Replicon-eGFP were con-transfected the next day. Protein expression was monitored under a fluorescence microscope at 48 hr post-transfection. Cell cultures were collected and subjected to one freeze/thaw cycle. Following centrifugation at 1700 × g for 5 min to remove cellular debris, PV1/Sabin and PV1/Mahoney pseudovirus stocks were obtained.

For pseudovirus titration, the pseudovirus stocks were serially diluted by ten-fold and added to wells (100 μL/well) of 96-well plates. Then, 100μL of suspended 293T cells ($4x10^4$ cells) was added to each well and incubated at 37°C with 5% CO_2 for 20 hr. After gently removing the medium, cells in the wells were analyzed by ImmunoSpotS6 (CTL) and the number of GFP fluorescent spots was counted. Pseudovirus titer was calculated as GFP fluorescent focus unit (FFU) per mL of the pseudovirus stock.

ARTICLE IN PRESS

Pseudovirus-based neutralization assay

Pseudovirus neutralization assay was conducted in a 96-well plate. Briefly, 50 μL of 2-fold serially diluted serum sample were mixed with equal volume of pseudovirus containing 200 FFU, followed by incubation at 37°C for 2 hr. Then, 4×10^4 293T cell were added to each well of the 96-well plate and incubated at 37°C with 5% CO_2. After 20 hr, the medium was gently removed, and the cells were examined for GFP fluorescent spots using the ImmunoSpotS6 plate reader. The neutralization titers were defined as the highest serum dilutions that inhibited at least 90% of GFP fluorescent focus formation.

Preparation of anti-PV1 monoclonal antibodies

Balb/c mice were injected intraperitoneally (i.p.) with 5 μg of PV1 sVLP plus 60 μg aluminum hydroxide at week 0, 2 and 4. About two weeks after the third immunization, one mouse was injected intravenously with 7 μg of PV1 sVLP in PBS. Three days after the boost, splenocytes were taken from the mouse and fused with SP2/0 myeloma cells using PEG 1450 (Sigma, USA), followed by HAT (Sigma) selection for 10 days. Next, hybridoma supernatants were screened by ELISA with PV1 sVLP as the coating antigen. Positive hybridomas were subcloned 2–4 times to generate monoclonal stable cell lines. Antibody isotypes were measured using SBA Clonotyping™ System/HRP ELISA kit (Southern Biotech, USA) according to manufacturer's protocol. Heavy and light chain variable region sequences were determined using the 5' RACE System (Invitrogen, USA) or mouse Ig-primer set (Novagen, Merck, Germany) according to the manufacturer's protocols and then analyzed using the IgBLAST tool[43].

MAbs were purified from ascites using protein G agarose resin 4FF (Yeasen, China) according to our previously described protocol [44]. Fabs were obtained by papain digestion of anti-PV1 MAbs and then purified using a HiTrap Capto DEAE column (Cytiva). The flow-through fraction containing the Fab fragments was collected, while the Fc fragments were eluted using a high-salt buffer (2.2 mM PBS supplemented with 500 mM NaCl). The Fab-containing fraction was concentrated using a 3 kDa molecular weight cut-off ultrafiltration device (Millipore).

ARTICLE IN PRESS

Bio-layer interferometry (BLI) assay

Prior to BLI analysis, purified PV1 sVLPs were labeled with EZ-Link™ Sulfo-NHS-LC-LC-Biotin (Thermo Fisher Scientific) and subsequently desalted using Zeba™ spin desalting columns (Thermo Fisher Scientific) according to the manufacturer's instructions. The binding affinities of mAbs to PV1 sVLPs were measured using an Octet® RED96 System (FortéBio, a Sartorius company, USA). Biotinylated sVLPs were immobilized onto streptavidin biosensors (FortéBio, Sartorius), followed by incubation with serial dilutions of mAbs to monitor the association phase. The sensors were then transferred into a dissociation buffer (10mM PBS containing 0.1% bovine serum albumin and 0.02% Tween-20) to record the dissociation phase. Equilibrium dissociation constants (KD) were calculated using Octet Data Analysis Software v11.0 (Sartorius).

Cryo-EM sample preparation and data collection

To prepare the cryo-EM samples of wtVLP and sVLP, a 2.4 µl aliquot of the sample was applied onto a plasma-cleaned lacey-carbon grid (Cu, 400 mesh, Ted Pella). Grids were blotted using Vitrobot Mark IV (Thermo Fisher Scientific) with a blot force of -1, blot time of 1 s, at 100% humidity and 8 °C, and plung-frozen in liquid ethane cooled by liquid nitrogen. For sVLP-3G10 sample, sVLP was incubated with 3G10 Fab (1:180 molar ratio) at room temperature for 30 min before freezing.

Cryo-EM movies were collected on a Titan Krios electron microscope (Thermo Fisher Scientific) operated at an accelerating voltage of 300kV. The movies for the two datasets were recorded at 64,000x a magnification in counting mode (yielding a pixel size of 1.093 Å), using a K3 directed electron detector (Gatan). Each frame was exposed for 0.1 s, with a total accumulation time of 3 s, leading to a total accumulated dose of 50.2 $e^{-}/Å^{2}$ on the specimen.

Cryo-EM single particle 3D reconstruction

Data processing procedure was consistent across all datasets. Motion correction was performed using Motioncor2 in Relion 4.0 [45,46], and CTF parameters were estimated with CTFFIND4 [47]. For wtVLP, 263,708 particles were auto-picked from 1,372 micrographs using crYOLO [48], with 211,442

ARTICLE IN PRESS

particles remained after reference-free 2D classification. These particles were refined using the PV2 wtVLP map (EMD-60095) as the initial model [23], followed by 3D auto-refinement with icosahedral symmetry. After CTF refinement, Bayesian polishing in Relion, and further refinement in cryoSPARC [49], a wtVLP map was obtained at a resolution of 2.95 Å. Similarly, sVLP processing produced a 2.43 Å resolution map from 48,710 particles. For sVLP-3G10, a 2.60 Å sVLP-3G10 map was obtained. Additionally, to enhance the local resolution of the 3G10 Fab and sVLP interface, symmetry expansion and local refinement were performed in cryoSPARC, yielding a final loal map at resolution of 2.83 Å. The overall resolutions were determined using the gold-standard Fourier shell correlation (FSC) 0.143 criterion [50]. Final maps were post-processed with deepEMhancer [51].

Atomic model building and analysis

We utilized the PV1 135S-like expanded particle model (PDB: 6P9O) [30] as initial model to build the homology model of wtVLP via SWISS-MODEL webserver [30,52]. For sVLP, the PV1 cryo-EM structures (PDB: 1HXS) [53] served as the initial model. Models were flexibly refined against their respective cryo-EM maps utilizing Rossetta [54]. Well-resolved side chain densities throughout our maps enabled comprehensive refinement in COOT [55]. We then used the phenix.real_space_refine module in Phenix for further refinement [56], and the final atomic models were validated using phenix.molprobity [57]. We conducted analyses of the interaction interface through the PISA server [58].

UCSF Chimera and ChimeraX were applied for figure generation and hydrophobic interaction surface analysis [59,60].

Statistics

All statistical analysis was performed using GraphPad Prism version 8. Neutralizing titers of the mouse sera from different immunization groups were compared by Mann-Whitney two-tailed test.

ARTICLE IN PRESS

Data availability

Cryo-EM maps have been deposited in the Electron Microscopy Data Bank (http://www.emdataresource.org) with the accession numbers of EMD-65817 for wtVLP，EMD-65818 for sVLP, and EMD-65819 for sVLP-3G10. The associated models have been deposited to the Protein Data Bank (https://www.rcsb.org/) with accession codes 9WAG, 9WAH, and 9WAI.

ARTICLE IN PRESS

ARTICLE IN PRESS

Acknowledgments

We are grateful to the staffs of the NCPSS Electron Microscopy Facility, Database and Computing Facility, and Protein Expression and Purification Facility for instrument support and technical assistance.

Funding

This work was supported by grants from the National Natural Science Foundation of China (32370991 to Z.H.), National Key R&D Program of China (2024YFA1803102 to Y.C.), the Shanghai Municipal Science and Technology Major Project (ZD2021CY001 to Z.H.), the Strategic Priority Research Program of CAS (XDB0570000 to Y.C.), the NSFC (32130056, 32570924 to Y.C.), and the Shanghai Pilot Program for Basic Research from CAS (JCYJ-SHFY-2022-008 to Y.C.). Q.H. was supported by the China National Postdoctoral Program for Innovative Talents (BX20250141).

ARTICLE IN PRESS

Author contribution

Z.H., Y.C., X.W. and Q.L. designed the experiments; T.C., W.H., S.W., C.Y.L. (Chaoyang Lian), Y.Z., L.R., T.W., and C.S. performed the biochemical and animal experiments. Q.H. collected the cryo-EM data and performed cryo-EM reconstructions and model building. C.L. involved in initial cryo-EM sample screen. Q.H., T.C. and W.H. analyzed the data. Z.H., Y.C., X.W., Q.L., Q.H. and T.C. wrote the manuscript.

Competing interests

W.H., C.L., L.R., Q.L. and X.W. are current employees of Huasong (Shanghai) Biomedical Technology Co., LTD. Q.L., X.W. L.R., T.C. and W.H. are inventors of a patent (CN 202410797193.1) on the 5C6 mAb owned by Huasong (Shanghai) Biomedical Technology Co., LTD. Q.L., X.W., L.R., C.Y.L., Z.H. and T.C. are listed as inventors in a pending patent application (CN 202511196350.4) on the 3G10 mAb filed by Huasong (Shanghai) Biomedical Technology Co.,

ARTICLE IN PRESS

LTD. The other authors declare that they have no competing interests.

ARTICLE IN PRESS

ARTICLE IN PRESS

References

1 Minor, P. D. An Introduction to Poliovirus: Pathogenesis, Vaccination, and the Endgame for Global Eradication. *Methods Mol Biol* **1387**, 1–10 (2016). https://doi.org/10.1007/978-1-4939-3292-4_1

2 Hogle, J. M. Poliovirus cell entry: common structural themes in viral cell entry pathways. *Annu Rev Microbiol* **56**, 677–702 (2002). https://doi.org/10.1146/annurev.micro.56.012302.160757

3 Kitamura, N. *et al.* Primary structure, gene organization and polypeptide expression of poliovirus RNA. *Nature* **291**, 547–553 (1981). https://doi.org/10.1038/291547a0

4 Hogle, J. M., Chow, M. & Filman, D. J. Three-dimensional structure of poliovirus at 2.9 A resolution. *Science* **229**, 1358–1365 (1985). https://doi.org/10.1126/science.2994218

5 Ypma-Wong, M. F., Dewalt, P. G., Johnson, V. H., Lamb, J. G. & Semler, B. L. Protein 3CD is the major poliovirus proteinase responsible for cleavage of the P1 capsid precursor. *Virology* **166**, 265–270 (1988). https://doi.org/10.1016/0042-6822(88)90172-9

6 Hindiyeh, M., Li, Q. H., Basavappa, R., Hogle, J. M. & Chow, M. Poliovirus mutants at histidine 195 of VP2 do not cleave VP0 into VP2 and VP4. *J Virol* **73**, 9072–9079 (1999). https://doi.org/10.1128/jvi.73.11.9072-9079.1999

7 Basavappa, R. *et al.* Role and mechanism of the maturation cleavage of VP0 in poliovirus assembly: structure of the empty capsid assembly intermediate at 2.9 A resolution. *Protein Sci* **3**, 1651–1669 (1994). https://doi.org/10.1002/pro.5560031005

8 Jacobson, M. F. & Baltimore, D. Morphogenesis of poliovirus. I. Association of the viral RNA with coat protein. *J Mol Biol* **33**, 369–378 (1968). https://doi.org/10.1016/0022-2836(68)90195-2

9 Hummeler, K. & Hamparian, V. V. Studies on the complement fixing antigens of poliomyelitis. I. Demonstration of type and group specific antigens in native and heated viral preparations. *J Immunol* **81**, 499–505 (1958).

10 Mayer, M. M. *et al.* The purification of poliomyelitis virus as studied by complement fixation. *Journal of immunology (Baltimore, Md. : 1950)* **78**, 435–455 (1957).

11 Le Bouvier, G. L. The modification of poliovirus antigens by heat and ultraviolet light. *Lancet* **269**, 1013–1016 (1955). https://doi.org/10.1016/s0140-6736(55)93435-8

12 Strauss, M., Schotte, L., Karunatilaka, K. S., Filman, D. J. & Hogle, J. M. Cryo-electron Microscopy Structures of Expanded Poliovirus with VHHs Sample the Conformational Repertoire of the Expanded State. *J Virol* **91** (2017). https://doi.org/10.1128/JVI.01443-16

13 Minor, P. Vaccine-derived poliovirus (VDPV): Impact on poliomyelitis eradication. *Vaccine* **27**, 2649–2652 (2009). https://doi.org/10.1016/j.vaccine.2009.02.071

14 Bandyopadhyay, A. S., Garon, J., Seib, K. & Orenstein, W. A. Polio vaccination: past, present and future. *Future Microbiol* **10**, 791–808 (2015). https://doi.org/10.2217/fmb.15.19

15 Connor, R. I. *et al.* Mucosal immunity to poliovirus. *Mucosal Immunol* **15**, 1–9 (2022). https://doi.org/10.1038/s41385-021-00428-0

16 Duizer, E., Ruijs, W. L., van der Weijden, C. P. & Timen, A. Response to a wild poliovirus type 2 (WPV2)-shedding event following accidental exposure to WPV2, the Netherlands, April 2017. *Euro Surveill* **22** (2017). https://doi.org/10.2807/1560-7917.ES.2017.22.21.30542

17 Roldao, A., Mellado, M. C., Castilho, L. R., Carrondo, M. J. & Alves, P. M. Virus-like particles in vaccine

ARTICLE IN PRESS

ARTICLE IN PRESS

development. *Expert Rev Vaccines* **9**, 1149–1176 (2010). https://doi.org/10.1586/erv.10.115

18 Kushnir, N., Streatfield, S. J. & Yusibov, V. Virus-like particles as a highly efficient vaccine platform: diversity of targets and production systems and advances in clinical development. *Vaccine* **31**, 58–83 (2012). https://doi.org/10.1016/j.vaccine.2012.10.083

19 Urakawa, T. *et al.* Synthesis of immunogenic, but non-infectious, poliovirus particles in insect cells by a baculovirus expression vector. *J Gen Virol* **70 (Pt 6)**, 1453 – 1463 (1989). https://doi.org/10.1099/0022-1317-70-6-1453

20 Jore, J. P. *et al.* Formation of poliomyelitis subviral particles in the yeast Saccharomyces cerevisiae. *Yeast* **10**, 907–922 (1994). https://doi.org/10.1002/yea.320100706

21 Rombaut, B., Jore, J. & Boeye, A. A competition immunoprecipitation assay of unlabeled poliovirus antigens. *J Virol Methods* **48**, 73–79 (1994). https://doi.org/10.1016/0166-0934(94)90090-6

22 Fox, H., Knowlson, S., Minor, P. D. & Macadam, A. J. Genetically Thermo-Stabilised, Immunogenic Poliovirus Empty Capsids; a Strategy for Non-replicating Vaccines. *PLoS Pathog* **13**, e1006117 (2017). https://doi.org/10.1371/journal.ppat.1006117

23 Hong, Q. *et al.* Vaccine Potency and Structure of Yeast-Produced Polio Type 2 Stabilized Virus-like Particles. *Vaccines (Basel)* **12** (2024). https://doi.org/10.3390/vaccines12091077

24 Marsian, J. *et al.* Plant-made polio type 3 stabilized VLPs-a candidate synthetic polio vaccine. *Nat Commun* **8**, 245 (2017). https://doi.org/10.1038/s41467-017-00090-w

25 Xu, Y. *et al.* Virus-like particle vaccines for poliovirus types 1, 2, and 3 with enhanced thermostability expressed in insect cells. *Vaccine* **37**, 2340–2347 (2019). https://doi.org/10.1016/j.vaccine.2019.03.031

26 Bahar, M. W. *et al.* Mammalian expression of virus-like particles as a proof of principle for next generation polio vaccines. *NPJ Vaccines* **6**, 5 (2021). https://doi.org/10.1038/s41541-020-00267-3

27 Sherry, L. *et al.* Production and Characterisation of Stabilised PV-3 Virus-like Particles Using Pichia pastoris. *Viruses* **14** (2022). https://doi.org/10.3390/v14102159

28 Sherry, L. *et al.* Recombinant expression systems for production of stabilised virus-like particles as next-generation polio vaccines. *Nat Commun* **16**, 831 (2025). https://doi.org/10.1038/s41467-025-56118-z

29 Miller, S. T., Hogle, J. M. & Filman, D. J. phasing of high-symmetry macromolecular complexes:: Successful phasing of authentic poliovirus data to 3.0 Å resolution. *Journal of molecular biology* **307**, 499–512 (2001). https://doi.org/10.1006/jmbi.2001.4485

30 Shah, P. N. M. *et al.* Cryo-EM structures reveal two distinct conformational states in a picornavirus cell entry intermediate. *PLoS Pathog* **16**, e1008920 (2020). https://doi.org/10.1371/journal.ppat.1008920

31 Strauss, M. *et al.* Nectin-like interactions between poliovirus and its receptor trigger conformational changes associated with cell entry. *J Virol* **89**, 4143–4157 (2015). https://doi.org/10.1128/JVI.03101-14

32 Sherry, L. *et al.* Production of an immunogenic trivalent poliovirus virus-like particle vaccine candidate in yeast using controlled fermentation. *NPJ Vaccines* **10**, 64 (2025). https://doi.org/10.1038/s41541-025-01111-2

33 Sherry, L. *et al.* Protease-Independent Production of Poliovirus Virus-like Particles in Pichia pastoris: Implications for Efficient Vaccine Development and Insights into Capsid Assembly. *Microbiol Spectr* **11**, e0430022 (2023). https://doi.org/10.1128/spectrum.04300-22

34 Minor, P. *et al.* Principal and subsidiary antigenic sites of VP1 involved in the neutralization of poliovirus type 3. *Journal of General Virology* **66**, 1159–1165 (1985).

ARTICLE IN PRESS

ARTICLE IN PRESS

35 Charnesky, A. J. *et al.* A human monoclonal antibody binds within the poliovirus receptor-binding site to neutralize all three serotypes. *Nat Commun* **14**, 6335 (2023). https://doi.org/10.1038/s41467-023-41052-9

36 Fiore, L. *et al.* Poliovirus Sabin type 1 neutralization epitopes recognized by immunoglobulin A monoclonal antibodies. *Journal of virology* **71**, 6905–6912 (1997). https://doi.org/10.1128/jvi.71.9.6905-6912.1997

37 Diamond, D. C. *et al.* Antigenic variation and resistance to neutralization in poliovirus type 1. *Science* **229**, 1090–1093 (1985).

38 Minor, P. D., Ferguson, M., Evans, D. M., Almond, J. W. & Icenogle, J. P. Antigenic structure of polioviruses of serotypes 1, 2 and 3. *J Gen Virol* **67 (Pt 7)**, 1283–1291 (1986). https://doi.org/10.1099/0022-1317-67-7-1283

39 Page, G. *et al.* Three-dimensional structure of poliovirus serotype 1 neutralizing determinants. *Journal of virology* **62**, 1781–1794 (1988).

40 Puligedda, R. D. *et al.* Characterization of human monoclonal antibodies that neutralize multiple poliovirus serotypes. *Vaccine* **35**, 5455–5462 (2017). https://doi.org/10.1016/j.vaccine.2017.03.038

41 Liu, Q. *et al.* Detection, characterization and quantitation of coxsackievirus A16 using polyclonal antibodies against recombinant capsid subunit proteins. *J Virol Methods* **173**, 115–120 (2011). https://doi.org/10.1016/j.jviromet.2011.01.016

42 Zhang, C. *et al.* High-yield production of recombinant virus-like particles of enterovirus 71 in Pichia pastoris and their protective efficacy against oral viral challenge in mice. *Vaccine* **33**, 2335–2341 (2015). https://doi.org/10.1016/j.vaccine.2015.03.034

43 Ye, J., Ma, N., Madden, T. L. & Ostell, J. M. IgBLAST: an immunoglobulin variable domain sequence analysis tool. *Nucleic acids research* **41**, W34–W40 (2013).

44 Yi, Y. *et al.* Identification of Human Norovirus GII.3 Blockade Antibody Epitopes. *Viruses* **13** (2021). https://doi.org/10.3390/v13102058

45 Zheng, S. Q. *et al.* MotionCor2: anisotropic correction of beam-induced motion for improved cryo-electron microscopy. *Nat Methods* **14**, 331–332 (2017). https://doi.org/10.1038/nmeth.4193

46 Scheres, S. H. RELION: implementation of a Bayesian approach to cryo-EM structure determination. *J Struct Biol* **180**, 519–530 (2012). https://doi.org/10.1016/j.jsb.2012.09.006

47 Rohou, A. & Grigorieff, N. CTFFIND4: Fast and accurate defocus estimation from electron micrographs. *J Struct Biol* **192**, 216–221 (2015). https://doi.org/10.1016/j.jsb.2015.08.008

48 Wagner, T. *et al.* SPHIRE-crYOLO is a fast and accurate fully automated particle picker for cryo-EM. *Commun Biol* **2**, 218 (2019). https://doi.org/10.1038/s42003-019-0437-z

49 Punjani, A., Rubinstein, J. L., Fleet, D. J. & Brubaker, M. A. cryoSPARC: algorithms for rapid unsupervised cryo-EM structure determination. *Nat Methods* **14**, 290–296 (2017). https://doi.org/10.1038/nmeth.4169

50 Scheres, S. H. & Chen, S. Prevention of overfitting in cryo-EM structure determination. *Nat Methods* **9**, 853–854 (2012). https://doi.org/10.1038/nmeth.2115

51 Sanchez-Garcia, R. *et al.* DeepEMhancer: a deep learning solution for cryo-EM volume post-processing. *Commun Biol* **4**, 874 (2021). https://doi.org/10.1038/s42003-021-02399-1

52 Biasini, M. *et al.* SWISS-MODEL: modelling protein tertiary and quaternary structure using evolutionary information. *Nucleic Acids Res* **42**, W252–258 (2014). https://doi.org/10.1093/nar/gku340

53 Miller, S. T., Hogle, J. M. & Filman, D. J. Ab initio phasing of high-symmetry macromolecular complexes: successful phasing of authentic poliovirus data to 3.0 A resolution. *J Mol Biol* **307**, 499–512 (2001).

ARTICLE IN PRESS

ARTICLE IN PRESS

https://doi.org/10.1006/jmbi.2001.4485

54 DiMaio, F. *et al.* Atomic-accuracy models from 4.5-A cryo-electron microscopy data with density-guided iterative local refinement. *Nat Methods* **12**, 361–365 (2015). https://doi.org/10.1038/nmeth.3286

55 Emsley, P. & Cowtan, K. Coot: model-building tools for molecular graphics. *Acta Crystallogr D Biol Crystallogr* **60**, 2126–2132 (2004). https://doi.org/10.1107/S0907444904019158

56 Adams, P. D. *et al.* PHENIX: a comprehensive Python-based system for macromolecular structure solution. *Acta Crystallogr D Biol Crystallogr* **66**, 213–221 (2010). https://doi.org/10.1107/S0907444909052925

57 Chen, V. B. *et al.* MolProbity: all-atom structure validation for macromolecular crystallography. *Acta Crystallogr D Biol Crystallogr* **66**, 12–21 (2010). https://doi.org/10.1107/S0907444909042073

58 Schlee, S. *et al.* Prediction of quaternary structure by analysis of hot spot residues in protein-protein interfaces: the case of anthranilate phosphoribosyltransferases. *Proteins* **87**, 815–825 (2019). https://doi.org/10.1002/prot.25744

59 Pettersen, E. F. *et al.* UCSF Chimera--a visualization system for exploratory research and analysis. *J Comput Chem* **25**, 1605–1612 (2004). https://doi.org/10.1002/jcc.20084

60 Goddard, T. D. *et al.* UCSF ChimeraX: Meeting modern challenges in visualization and analysis. *Protein Sci* **27**, 14–25 (2018). https://doi.org/10.1002/pro.3235

ARTICLE IN PRESS

ARTICLE IN PRESS

Figure legends

Fig. 1. Expression of PV1 wtVLP and sVLP in *Pichia pastoris*. (**a**) Diagrams of the expression vectors. TRP2-L and TRP2-R, the up- and down-stream parts of the TRP region; P_{AOX1}, AOX1 promoter; CYC1 TT, CYC1 transcription termination region; ADE2, expression cassette encoding phosphoribosylaminoimidazole carboxylase, used as the selection marker. (**b**) SDS-PAGE and western blot analysis of the purified PV1 wtVLP and sVLP. The primary antibodies used in the western blot assays were indicated. (**c**) Visualization of *P. pastoris*-derived VLPs by negative stain electron microscopy. Bar=100 nm.

Fig. 2. Antigenic characterization of yeast-produced PV1 wtVLP and sVLP. (**a**) Reactivity of wtVLP and sVLP with anti-PV1 polyclonal antibody (pAb) or mAb234 in ELISA. (**b**) D antigen levels in the wtVLP or sVLP preparations. The data are means $\pm$ SD from three independent measurements. (**c**) Thermostability of PV1 sVLP. Equal amounts of PV1 sVLP were subjected to incubation at different temperatures for 10 min and then analyzed by ELISA using the pAb or mAb234. The red dash line and dotted line indicate the mAb234 reactivity (OD450nm values) corresponding to 50% and 10% of the D-antigen in the untreated VLPs, respectively. Representative data from two independent experiments were shown.

Fig. 3. **Immunogenicity of PV1 wtVLP and sVLP in mice.** (**a**) Mouse immunization and sampling schedule. (**b**) Neutralizing titers of the week-4 (post-2nd dose) and the week-6 (post-3rd dose) antisera against PV1/Sabin1 live virus. Serum samples that exhibited less than 50% neutralization at the lowest serum dilution (1:16) were assigned a titer of 8 for computation of geometric means. (**c**) Neutralizing titers of the week-4 (post-2nd dose) and the week-6 (post-3rd dose) antisera against PV1/Sabin1 pseudovirus. Serum samples that exhibited less than 90% neutralization at the lowest serum dilution (1:16) were assigned a titer of 8 for computation of geometric means. Each symbol represents one mouse. The geometric mean titer for each group was shown. Statistical significance between two groups was calculated by Mann-Whitney two-tailed test. ns, no significant difference ($p \geqslant 0.05$); *, $p<0.05$; **, $p<0.01$; ***, $p<0.001$; ****, $p<0.0001$.

Fig. 4. Cryo-EM structures of PV1 wtVLP and sVLP. (**a-b**) Cryo-EM density maps of wtVLP (a) and sVLP (b), viewed along the 2-fold axis, with the color bar indicating radius (in Å). (**c-d**) Central section of wtVLP (c) and sVLP (d) cryo-EM maps. (**e**) Model-to-map fitting for a single asymmetric unit, with VP1 (blue), VP2 (green), and VP3 (red). (**f**) Zoomed-in view of wtVLP and sVLP near the 2-fold symmetry axis.

ARTICLE IN PRESS

Fig. 5. Structural analysis of VLPs. (**a**) Asymmetric unit model of sVLP, with mutations shown as yellow spheres. (**b**) Overlay of the asymmetric units of PV1 SC6b yeast D particle (hot pink, PDB: 9EYY) and sVLP (in colors). (**c–e**) Superposition of VP1 (c), VP2 (d), and VP3 (e) for SC6b yeast D particle (hot pink) and sVLP (in colors). (**f**) Structural comparison of sVLP (in blue) with PV1 SC6b yeast D particle structure (PDB: 9EYY, in gray). (**g**) Overlay of the asymmetric units of PV1 SC6b yeast C particle (gray, PDB: 9EZ0) and wtVLP (in colors). (**h**) Overlay of the asymmetric units of PV1 SC6b mammalian C particle (light pink, PDB: 9F0K) and wtVLP (in colors).

Fig. 6. Identification of mAb 3G10 as a PV1 D-antigen-specific antibody. (**a**) Summary of mAb characteristics. (**b**) Reactivity of the mAbs to PV1 sVLP in ELISA. (**c**) Reactivity of the mAbs to PV1 wtVLP. (**d**) Side-by-side comparison of mAb234 and 3G10 in PV1 sVLP thermostability analysis. The purple dash line and the dotted line indicate the mAb234 reactivity (OD450 nm values) corresponding to 50% and 10% of the unheated PV1 sVLP antigen. The red dash line and the dotted line indicate the 3G10 reactivity (OD450 nm values) corresponding to 50% and 10% of the unheated PV1 sVLP antigen. (**e**) Binding kinetics of the mAb 3G10 to immobilized PV1 sVLP was measured by bio-layer interferometry (BLI). (**f-g**) Competitive ELISA. PV1 sVLP-coated wells were firstly incubated with different concentrations of the indicated mAbs, followed by detection with HRP-conjugated 3G10. The red dash line and the dotted line indicate the HRP-conjugated 3G10 reactivity (OD450 nm values) corresponding to 100% and 50% of the PV1 sVLP antigen.

Fig. 7. Cryo-EM structure of sVLP in complex with 3G10 Fab. (**a**) Cryo-EM density map of the sVLP-3G10 Fab complex, viewed along the 2-fold axis, with the color bar indicating radius (in Å). (**b**) Model-to-map fitting of the composite sVLP-3G10 complex, with a zoomed-in view of VP1/VP2–3G10 interactions (HC: heavy chain; LC: light chain). (**c**) Binding Interface between sVLP protomer and 3G10 Fab. (**d**) Zoomed-in views of regions boxed in (c), showing interactions between VP1 BC, VP1 GH, and VP2 EF loops of sVLP and 3G10 Fab CDR regions (Spring: salt bridges; black dashed line: hydrogen bond). (**e**) Structural comparison of sVLP-3G10 and sVLP, revealing slight conformational changes in VP2 EF loop and VP1 GH loop. (**f**) Roadmap illustrating the footprints of 3G10 Fab and PVR receptor on the sVLP surface, generated using RIVEM (Radial Interpretation of Viral Electron density Maps). Polar angles θ and φ represent latitude and longitude, respectively. Viral residues are colored according to the radius. The color bar indicates the corresponding radius (unit in Å). Footprint of 3G10 Fab and the PVR receptor (PDB: 3J8F) are also shown in orange and white, respectively.

ARTICLE IN PRESS

Fig. 8. Conservation analysis of the 3G10 epitope and double-mAb sandwich ELISA for PV1 D-antigen measurement. (**a**) Sequence alignment showing that the 3G10 epitope is identical among the wildtype Mahoney, the Mahoney-SC7, and the Sabin-1 strains. The key residues of the 3G10 epitope are indicated by red arrowheads. (**b**) Reactivities of serially diluted cIPV international standard detected by sandwich ELISAs with rabbit anti-PV1 pAb as the capture antibody and the indicated mAbs as the detection antibody. The X-axis shows the amounts of PV1 D-antigen in diluted cIPV samples and is in log10 scale. (**c**) Reactivities of serially diluted cIPV international standard detected by sandwich ELISAs with 5C6 as the capture antibody and HRP-conjugated 3G10 (3G10-HRP) as the detection antibody. The X-axis shows the amounts of PV1 D-antigen in diluted cIPV samples and is in log10 scale. (**d**) Standard curve generated by the 5C6/3G10-HRP based sandwich ELISA with the international cIPV as reference. The raw data are the same as in (c) but was re-plotted with X-axis in linear scale.

ARTICLE IN PRESS

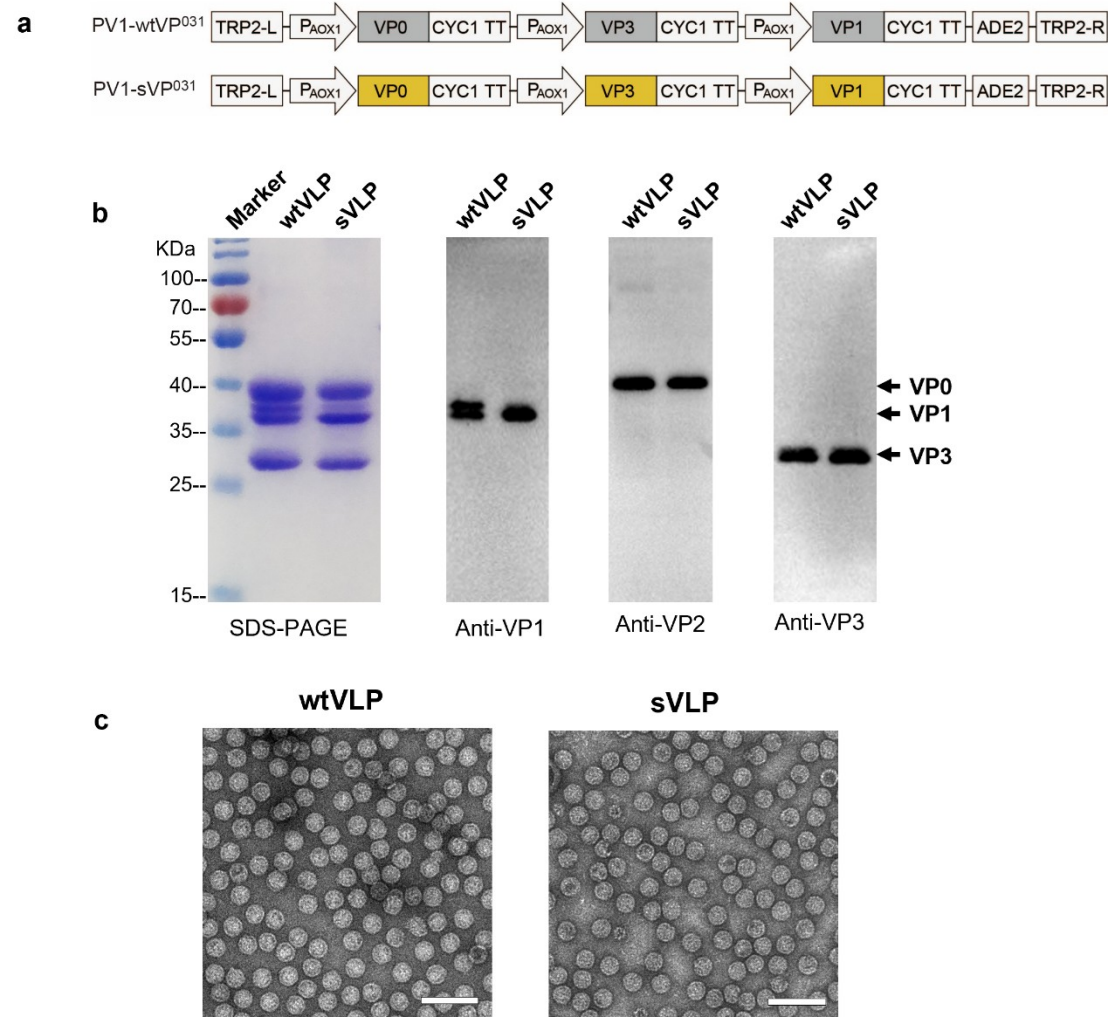
a
PV1-wtVP031
TRP2-L
PAOX1
VP0
CYC1 TT
PAOX1
VP3
CYC1 TT
PAOX1
VP1
CYC1 TT
ADE2
TRP2-R
PV1-sVP031
TRP2-L
PAOX1
VP0
CYC1 TT
PAOX1
VP3
CYC1 TT
PAOX1
VP1
CYC1 TT
ADE2
TRP2-R
b
Marker
wtVLP
sVLP
KDa
100--
70--
55--
40--
35--
25--
15--
SDS-PAGE
wtVLP
sVLP
Anti-VP1
wtVLP
sVLP
Anti-VP2
wtVLP
sVLP
VP0
VP1
VP3
Anti-VP3
c
wtVLP
sVLP

a

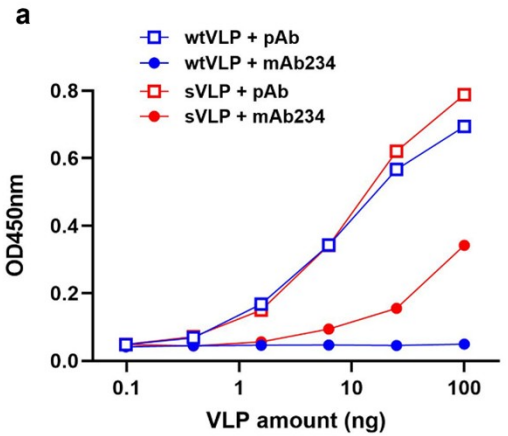

c

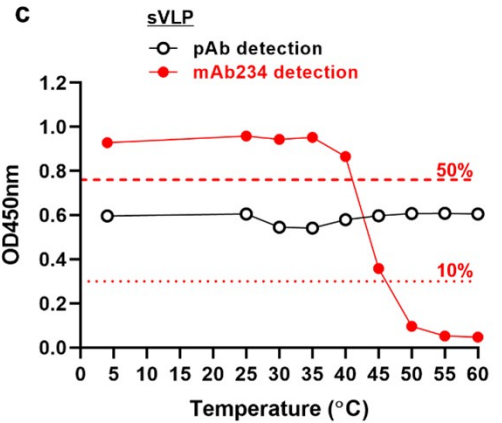

b

VLP type	D antigen unit per μg VLP (DU/ μg)
PV1 wtVLP	---
PV1 sVLP	187±17

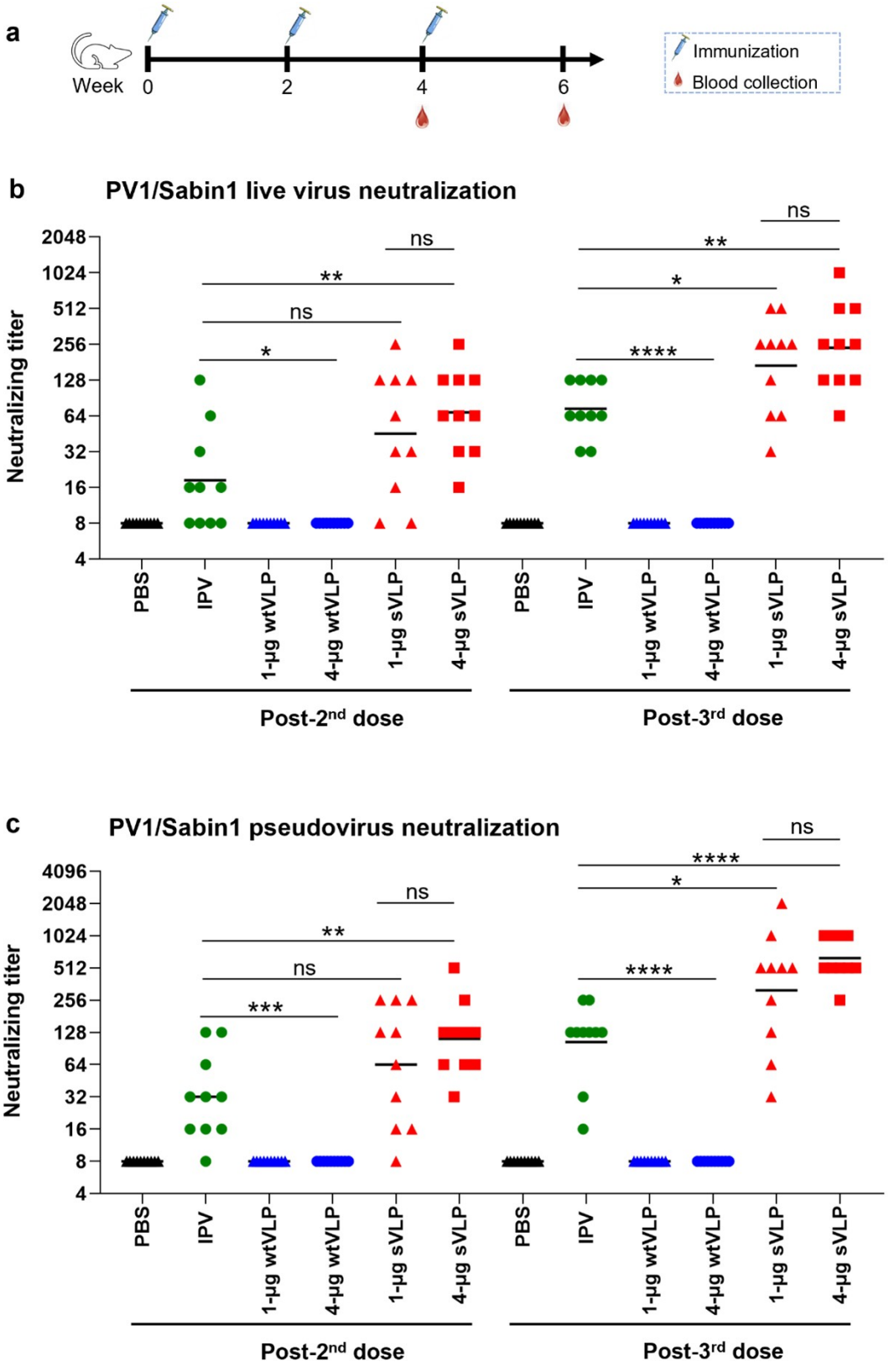
a
Week 0
2
4
6
Immunization
Blood collection
b
PV1/Sabin1 live virus neutralization
Neutralizing titer
2048
1024
512
256
128
64
32
16
8
4
ns
**
ns
*
ns
**
*
****
PBS
IPV
1-μg wtVLP
4-μg wtVLP
1-μg sVLP
4-μg sVLP
Post-2nd dose
Post-3rd dose
c
PV1/Sabin1 pseudovirus neutralization
Neutralizing titer
4096
2048
1024
512
256
128
64
32
16
8
4
ns
**
ns
***
ns
****
*
****
PBS
IPV
1-μg wtVLP
4-μg wtVLP
1-μg sVLP
4-μg sVLP
Post-2nd dose
Post-3rd dose

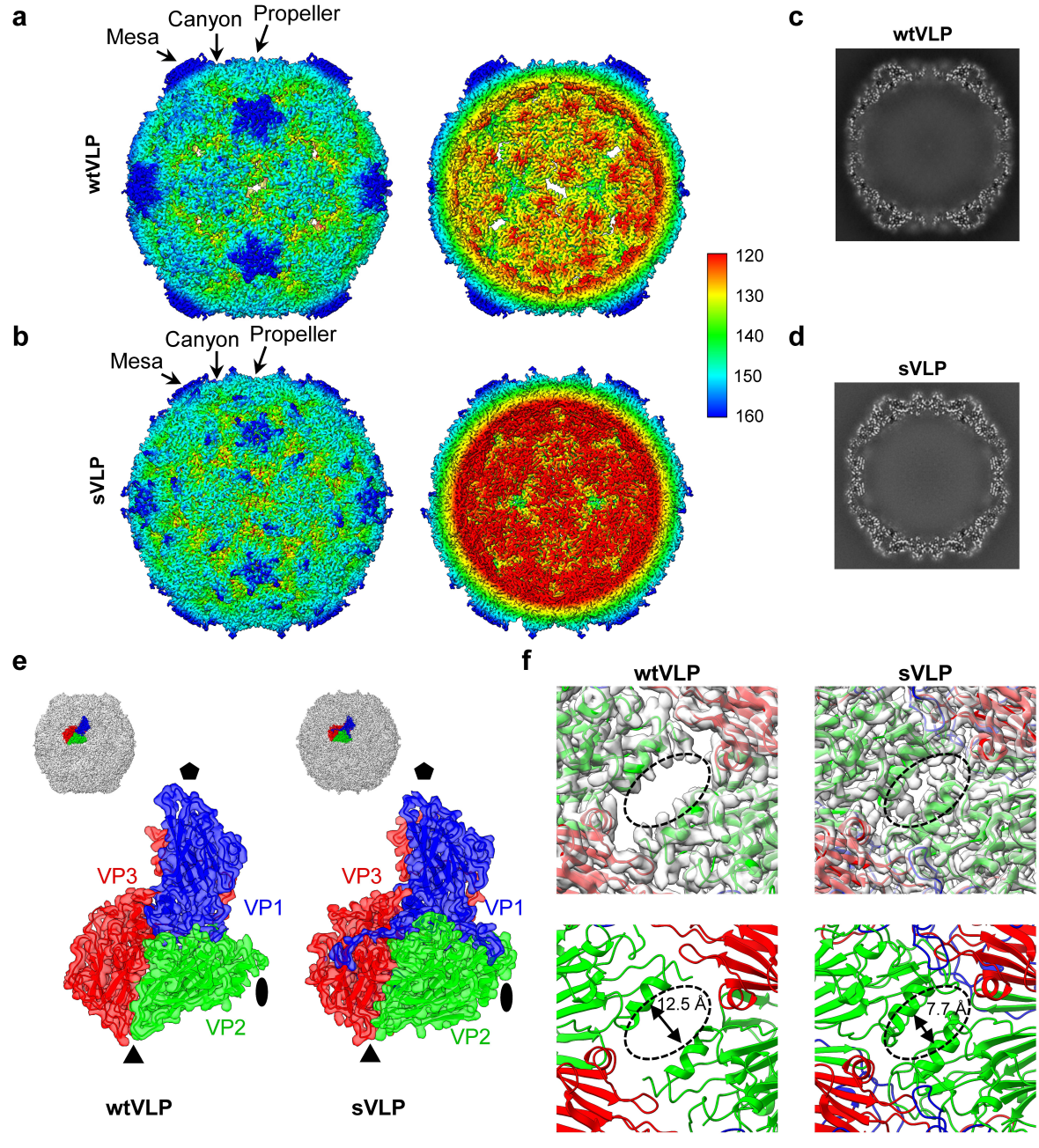
a
Mesa
Canyon
Propeller
wtVLP
120
130
140
150
160
b
Canyon
Propeller
Mesa
sVLP
c
wtVLP
d
sVLP
e
VP3
VP1
VP2
wtVLP
VP3
VP1
VP2
sVLP
f
wtVLP
sVLP
12.5 Å
7.7 Å

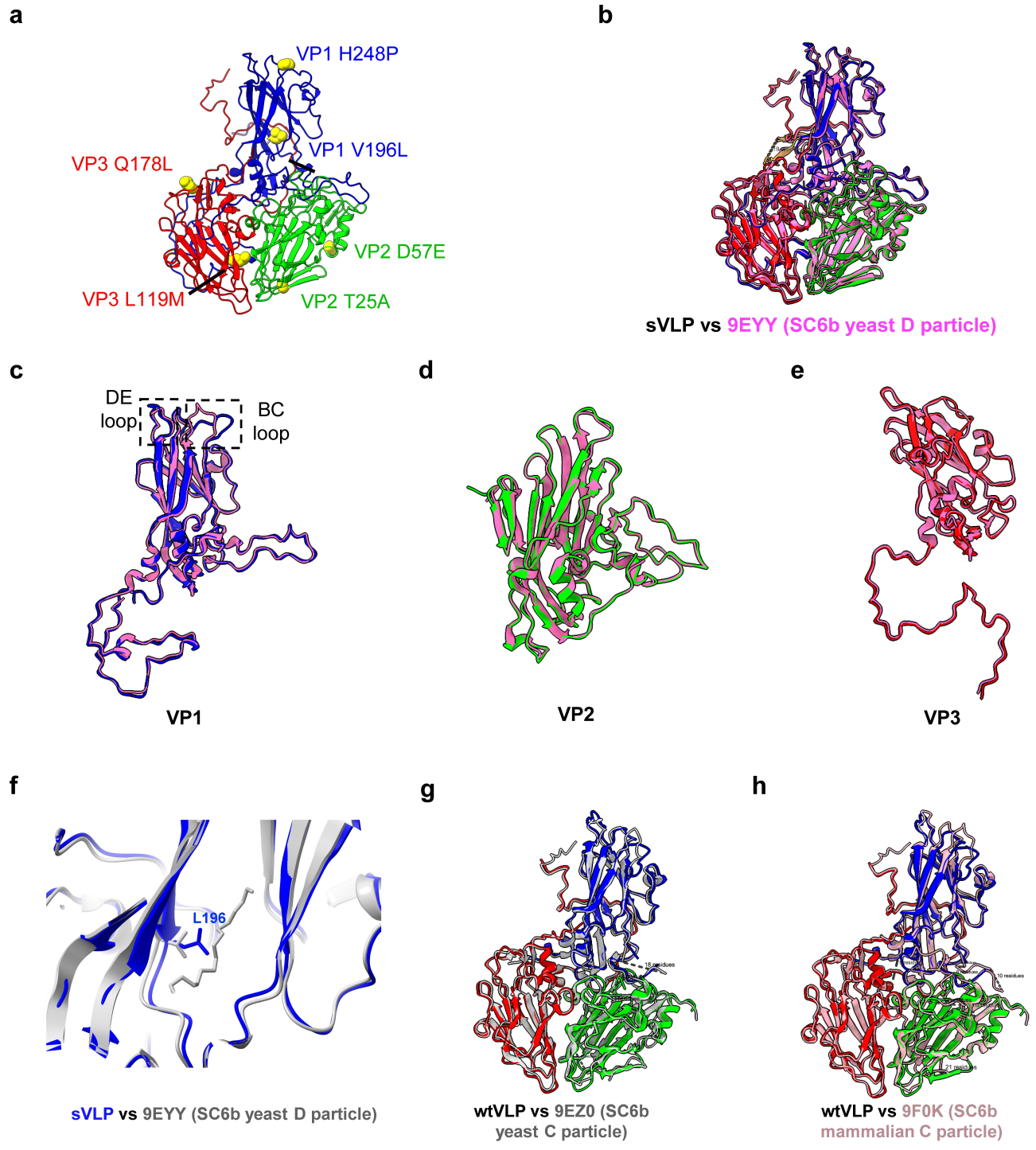
a
VP1 H248P
VP1 V196L
VP3 Q178L
VP2 D57E
VP3 L119M
VP2 T25A
b
sVLP vs 9EYY (SC6b yeast D particle)
c
DE loop
BC loop
VP1
d
VP2
e
VP3
f
L196
sVLP vs 9EYY (SC6b yeast D particle)
g
wtVLP vs 9EZ0 (SC6b yeast C particle)
h
wtVLP vs 9F0K (SC6b mammalian C particle)

a

mAb	Isotype	PV1 sVLP binding	PV1 wtVLP binding	Binding affinity to PV1 sVLP (nM)	Neutralization IC50 (μg/mL)	Pseudovirus neutralization IC90 (μg/mL)	
					Sabin1 (live)	Sabin1	Mahoney
3G10	IgG2a	+	-	0.53	0.016	0.006	0.006
5C6	IgG2b	+	+	ND	18.75	25	25

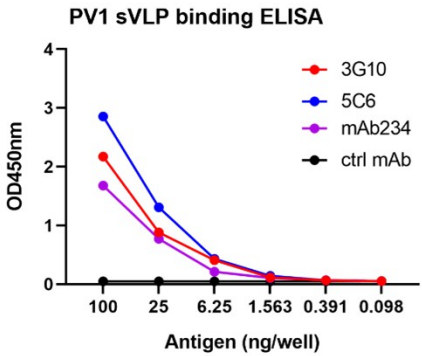

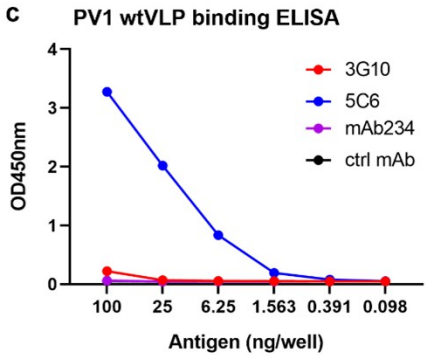

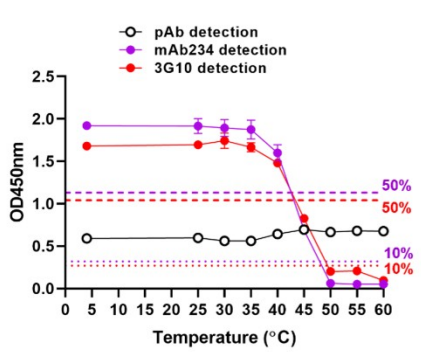

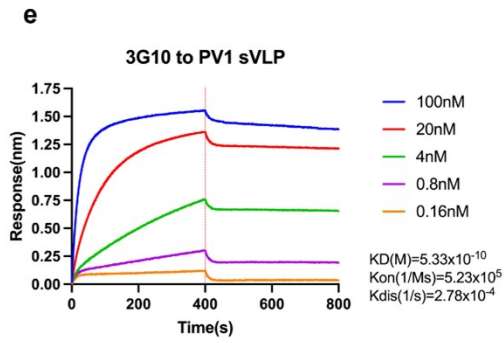

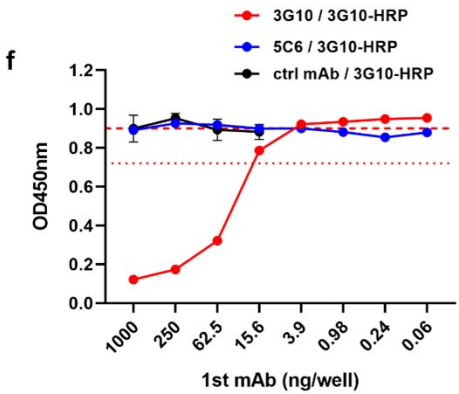

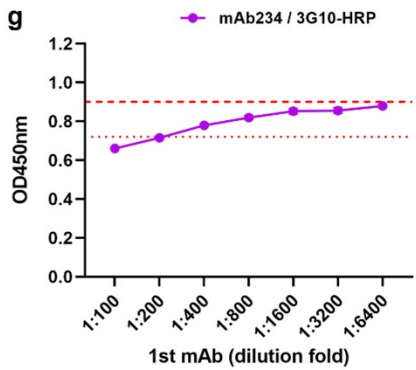

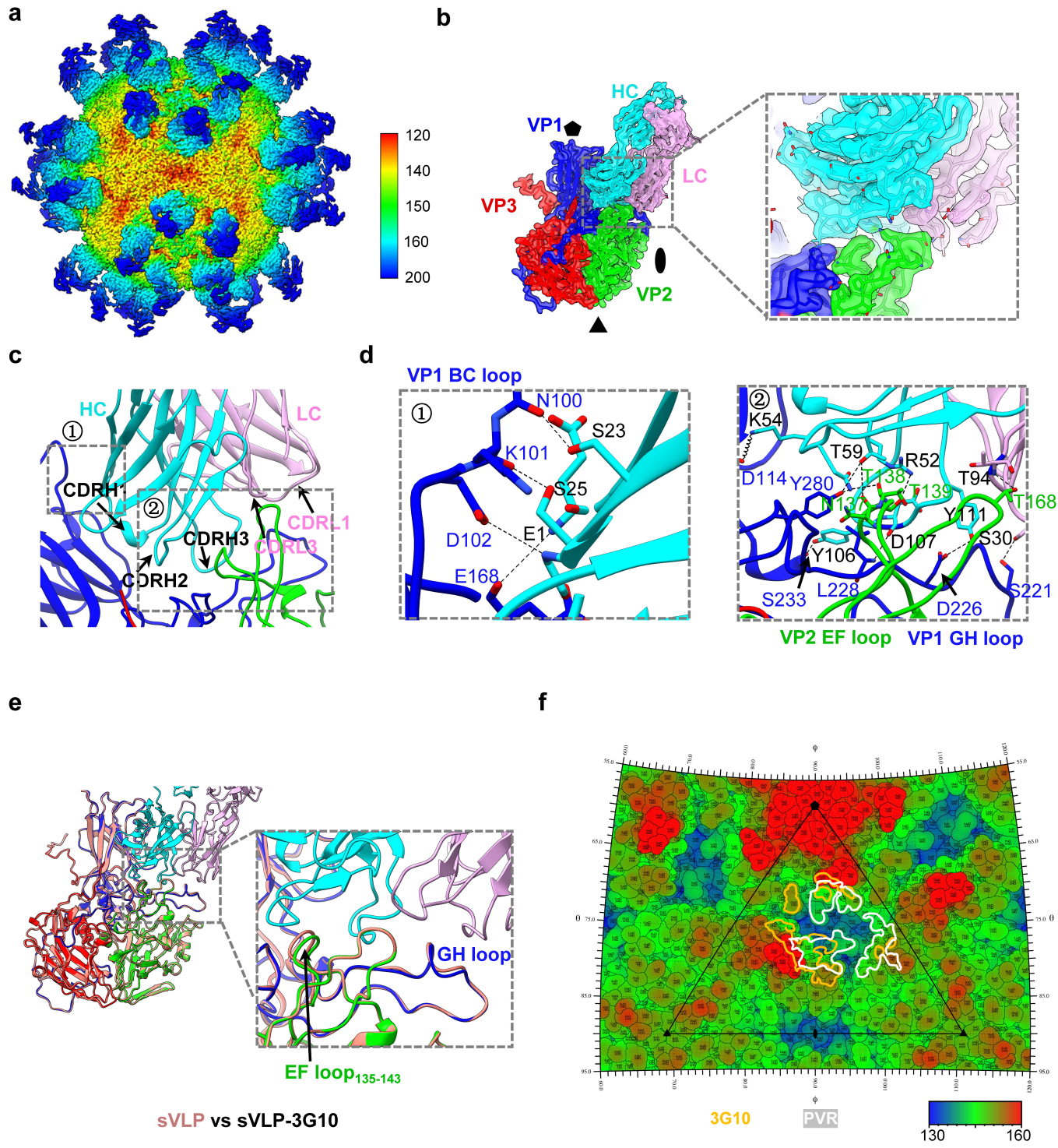
a
120
140
150
160
200
b
HC
VP1
LC
VP3
VP2
c
HC
LC
①
②
CDRH1
CDRL1
CDRH3
CDRL3
CDRH2
d
VP1 BC loop
①
N100
S23
K101
S25
D102
E1
E168
②
K54
T59
R52
D114
Y280
T138
T94
T139
T168
Y111
D107
S30
Y106
S233
L228
D226
S221
VP2 EF loop
VP1 GH loop
e
GH loop
EF loop135-143
sVLP vs sVLP-3G10
f
3G10
PVR
130
160

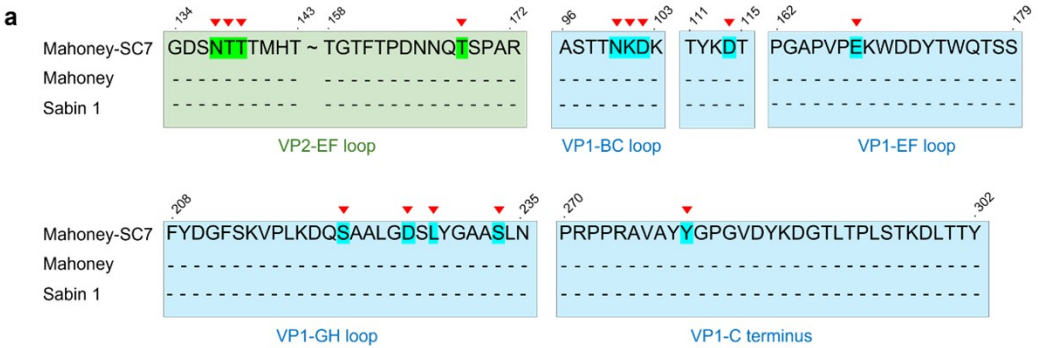
a
134
143
158
172
Mahoney-SC7
GDSNTTTMHT ~ TGTFTPDNNQTSPAR
Mahoney
Sabin 1
VP2-EF loop
96
103
111
115
ASTTNKDK
TYKDT
VP1-BC loop
162
179
PGAPVPEKWDDYTWQTSS
VP1-EF loop
208
235
FYDGFSKVPLKDQSAALGDSLYGAASLN
VP1-GH loop
270
302
PRPPRAVAYYGPGVDYKDGTLTPLSTKDLTTY
VP1-C terminus

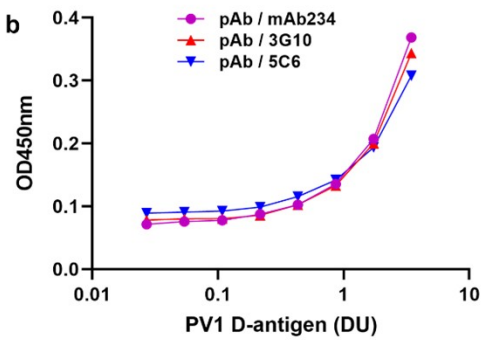
b
pAb / mAb234
pAb / 3G10
pAb / 5C6
OD450nm
PV1 D-antigen (DU)

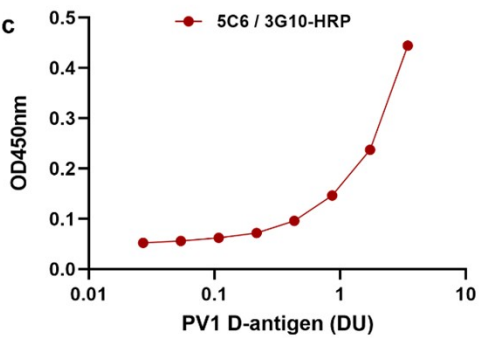
c
5C6 / 3G10-HRP
OD450nm
PV1 D-antigen (DU)

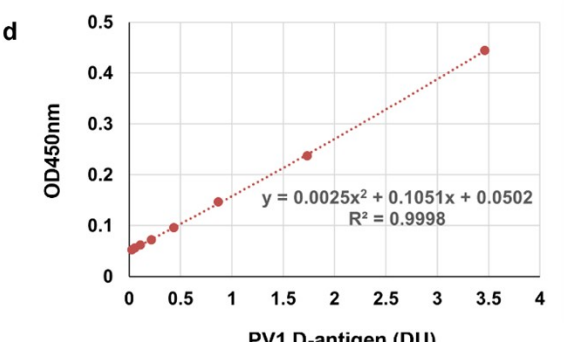
d
OD450nm
y = 0.0025x² + 0.1051x + 0.0502
R² = 0.9998
PV1 D-antigen (DU)